target specificity (26). We therefore introduced a point mutation at position 10 from the 3′-end of both MBSs (S-TuD-miR21-10mut). Base pair formation between the two MBSs of S-TuD-miR21-10mut was greatly reduced compared with that of S-TuD-miR21-pf (Supplementary Figure S3). When the miRNA inhibitory effects of S-TuD-miR21-pf, S-TuD-miR21-4ntin and S-TuD-miR21-10mut were tested (Figure 3A), S-TuD-miR21-10mut was found to be much more efficient. In the case of miR-200c, however, S-TuD-miR200c-pf was found to be a more potent inhibitor than S-TuD-miR200c-10mut (Figure 3B). This is possibly because neither S-TuD-miR200c-pf nor S-TuD-miR200c-10mut forms significant base pairing between the two MBSs. In such cases, a point mutation would reduce the inhibitory effects of the S-TuD, because of a lower binding affinity between the miRNA and MBSs.

If the above hypothesis was correct, we expected to see a clear difference between the secondary structure of S-TuD-miR21-pf and S-TuD-miR21-10mut (or S-TuD-miR21-4ntin). To test this, we measured the UV-melting curves of these three S-TuDs at 260 nm. As shown in Figure 4, the curves of S-TuD-miR21-10mut and S-TuD-miR21-4ntin were very similar and had two T_m (melting temperature) values of around 30–34°C and 70°C. In contrast, T_m values of 50°C and 70°C were observed for S-TuD-miR21-pf. Since a T_m at 70°C was observed in all three of these S-TuDs, this would represent a dissociation of the 18 bp stem I. A T_m at 30–34°C for S-TuD-miR21-10mut and S-TuD-miR21-4ntin would mainly reflect the dissociation of the 10 bp stem II. The gradual increase in UV absorbance at around 30–45°C and the rather large and sharp sigmoid curve at 50°C observed for S-TuD-miR21-pf reflects the secondary structure formed between the two MBSs of S-TuD-miR21-pf in addition to the base pairing of stem II. These thermal denaturation analyses thus support the idea that the interaction between the two MBSs of S-TuD-miR21-pf is significantly higher than those of S-TuD-miR21-4ntin and S-TuD-miR21-10mut.

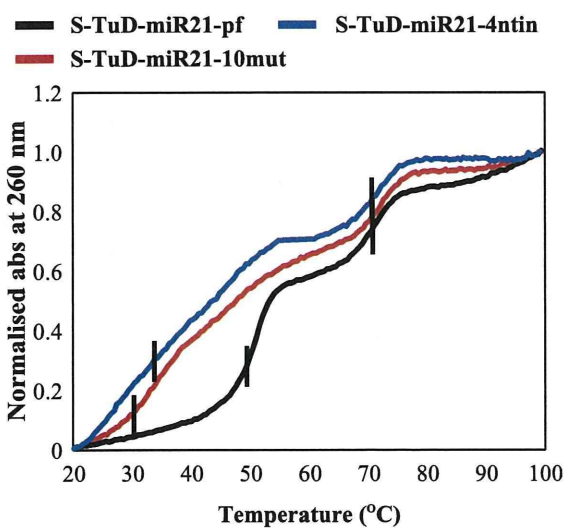

Figure 4. Normalized UV melting curves for 1.5 μM concentrations of S-TuD-miR21-pf, S-TuD-miR21-4ntin and S-TuD-miR21-10mut in a 10 mM sodium phosphate (pH 7.0) buffer containing 10 mM NaCl. Melting was assessed by UV absorbance at 260 nm and a melting rate of 0.5°C/min. Vertical black bars indicate the T_m points.

Taken together, these results suggest that to design an efficient S-TuD molecule in general, the two MBS regions should not form base pairs to a threshold level. If an MBS that is perfectly complementary to miRNA cannot satisfy this requirement, the introduction of a point mutation in the middle region or a 4-nt insertion would be one possible way to improve the inhibitory effects of the S-TuD molecule in question, even with the possible loss of binding affinity to the miRNA. For example, in the case of S-TuD-miR16-pf, S-TuD-miR16-4ntin and S-TuD-miR16-10mut (Supplementary Figure S3), the MBSs of which do not form strong base pairing, S-TuD-miR16-pf was shown to be the most efficient inhibitor as expected, when tested by the miR-16 luciferase reporter system (Figure 3C). From these experimental results, we roughly expect that the threshold number of base pairs between the two MBSs (plus 3-nt linkers at their both ends) is about nine, as predicted by CentroidFold.

In our previous report, the length of stem I was designed to be more than 16 bp and fixed at 18 bp in most cases so that the TuD RNA molecules synthesized in the nuclei can be efficiently transported into the cytoplasm (19,27). Since S-TuD is directly introduced into the cytoplasm by transfection, a long stem I structure is likely not to be required. To test this, we synthesized two S-TuDs with shorter stem I lengths of 14 and 10 bp, (S-TuD-miR21-10mut-14 bp and S-TuD-miR21-10mut-10 bp, respectively) (Supplementary Figure S4A) and compared their potency against the parental S-TuD molecule, S-TuD-miR21-10mut. The inhibitory effects of S-TuD-miR21-10mut-14 bp were slightly reduced and those of S-TuD-miR21-10mut-10 bp were considerably lower when compared with S-TuD-miR21-10mut (Supplementary Figure S4B). This indicated that an 18 bp Stem I contributes to inhibitory potency. To further understand the molecular mechanisms underlying this phenomenon, we analyzed the UV-melting curves of these three S-TuDs at 260 nm (Supplementary Figure S4C). As described in the previous section, the two T_m values for S-TuD-miR21-10mut were calculated at 34°C and 70°C, which reflect the dissociation of the 10 bp length stem II and 18 bp length stem I, respectively.

The T_m at 32°C for S-TuD-miR21-10mut-stemI-14 bp and at 37°C for S-TuD-miR21-10mut-stemI-10 bp likely reflect the dissociation of a single 10 bp stem II and two 10 bp stems of Stems I and II, respectively. This result suggests that the two strands comprising S-TuD-miR21-10mut-stemI-10 bp would at least partly dissociate from each other in cells at 37°C, consistent with the observation that the inhibitory effects of this molecule are severely affected (See Supplementary Figure S4B). Furthermore, a T_m at 57°C for S-TuD-miR21-10mut-stemI-14 bp, reflecting the dissociation of a 14 bp stem I, reveals that its S-TuD structure is not fully thermodynamically stable. These results thus show that an 18 bp length stem I

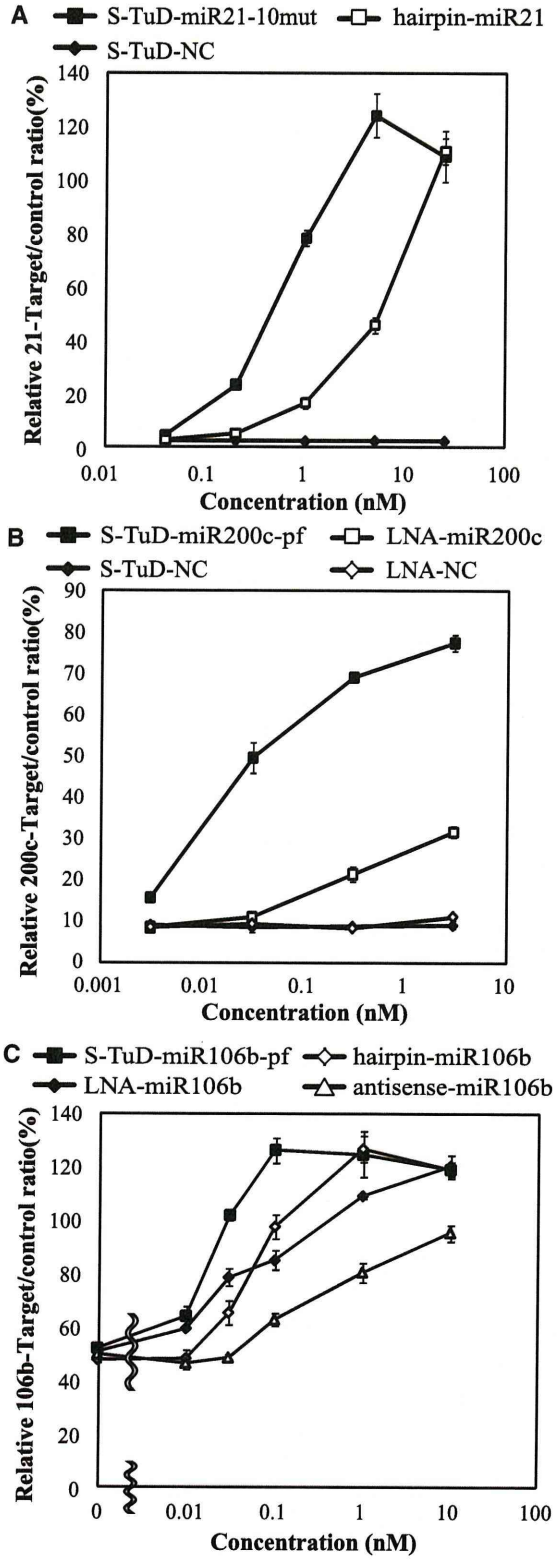

Figure 5. Dose-dependency of S-TuD-miR-21-10mut (**A**), S-TuD-miR-200c-pf (**B**) or S-TuD-miR-106b-pf (**C**) miRNA inhibitory activities. HCT-116 cells were transfected using similar procedures to those shown in Figure 3. (**A**) A dual luciferase assay was performed 48 h after transfection into HCT-116 cells and the miRNA hairpin inhibitor-miR21 was used for comparison. The expression ratios of miR-21-RL/FL to UT-RL/FL are represented by the mean ± SD (n = 3). (**B**) A dual luciferase assay was performed 48 h after transfection into HCT-116 cells. The LNA-inhibitor-miR200c was used for comparison. The ratios of miR-200c-RL/FL to UT-RL/FL expression are represented by the mean ± SD (n = 3). (**C**) A dual luciferase assay was performed 48 h after transfection into HCT-116 cells. Antisense-miR-106b, miRNA hairpin inhibitor-miR106b and LNA-inhibitor-miR106b were used for comparison. The ratios of miR-106b-RL/FL to UT-RL/FL are represented by the mean ± SD (n = 3) as the expression levels.

structure strongly contributes to the stabilization of the two stems that form the S-TuD structure and support the potent inhibitory activity of this molecule.

Dose dependency of S-TuD inhibitory activity

We next determined the dose–response curves of the S-TuDs targeting miR-21, miR-200c and miR-106b. The dose dependency of S-TuD-miR21-10mut as well as that of 2′-*O*-methylated RNA-based miRNA hairpin inhibitor-miR-21 was first determined (Figure 5A). S-TuD-miR21-10mut showed inhibitory effects at a concentration of 0.2 nM. At a concentration of 5 nM, the luciferase activity reached saturation, which almost corresponded to the levels of the reporter without the target sequence. On the other hand, miRNA hairpin inhibitor-miR-21 showed inhibitory effects at a concentration of 1 nM and saturation had not been reached as a concentration of 25 nM.

We next determined the dose dependency of S-TuD-miR200c-pf and of the LNA oligonucleotide antisense inhibitor targeting miR-200c (Figure 5B). S-TuD-miR200c-pf showed inhibitory effects at 0.003 nM which were saturated at 0.3 nM, whereas the effects of LNA-miR200c did not reach saturation even at 3 nM. Finally, we tested S-TuD-miR106b-pf as well as miRNA hairpin inhibitor and both LNA and 2′-*O*-methylated RNA antisense oligonucleotides, all of which are designed to target miR-106b (Figure 5C). S-TuD-miR106b-pf showed inhibitory effects at 0.01 nM which reached saturation at 0.1 nM. LNA-miR106b also showed inhibitory effects at 0.01 nM, but its saturation point was not reached even at 1 nM. The miRNA hairpin inhibitor-miR-106b showed inhibitory effects at 0.03 nM and reached saturation at 1 nM. 2′-*O*-methylated RNA antisense-miR106b oligonucleotides showed inhibitory effects at 0.1 nM but these remained low even at a concentration of 1 nM. We next determined levels of free miR-106b in cells introduced with these inhibitors using real-time PCR in a parallel cell culture treated with 0.05 nM of the inhibitors. At this dosage, relative target/control is expected to be significantly different among these four inhibitors. The free miR-106b levels determined are in the reverse order to the luciferase activity of these inhibitors (Supplementary Figure S5). We think the apparently high amount of free miR-106b even in S-TuD-miR106b-pf treated cells is partly reflecting that transfection efficiency of inhibitors at a low concentration

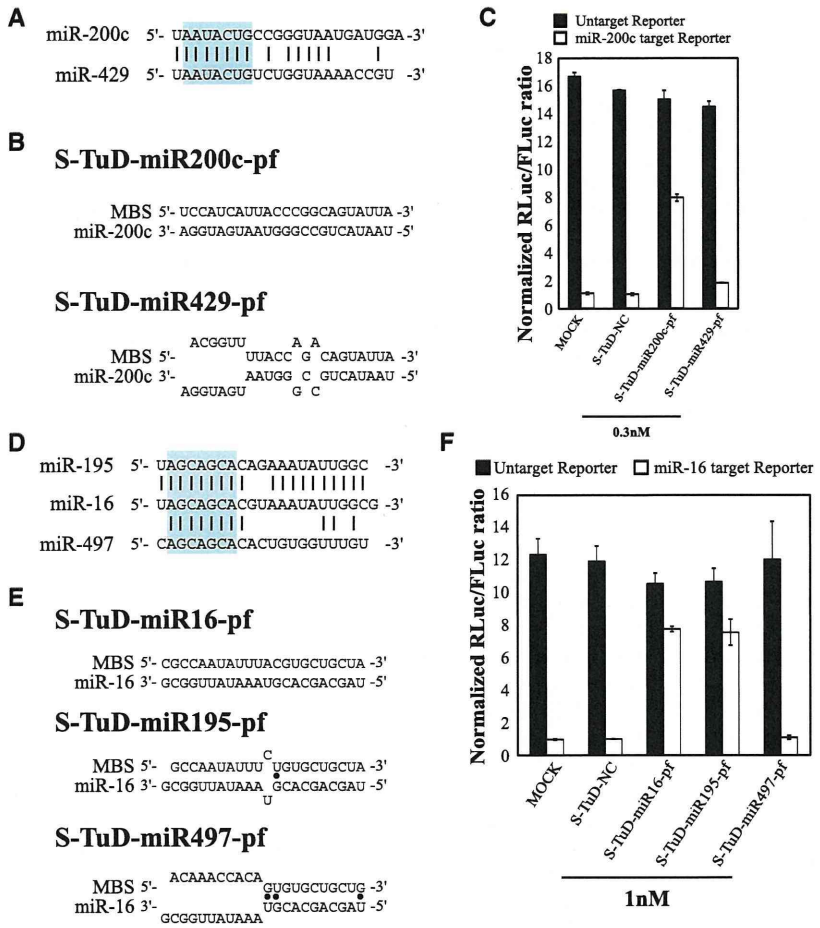

Figure 6. Inhibitory effects of S-TuD on related miRNAs. (**A**) miR-200c and -429 sequences and **(D)** miR-16,-195 and -497 sequences, and the degree of homology between them. Sequences shown in blue box are the heptameric seed sequence (2–8 nt from the 5′-end). Black bars indicated homologous nucleotides. Imperfect pairing between **(B)** miR-200 c and **(E)** miR-16 and MBSs of the corresponding S-TuD. Black dots indicate G-U pairs. (**C, F**) S-TuDs were transfected into HCT-116 cells together with the *Renilla* luciferase (C) miR-200c and (F) miR-16 reporter (open bars) or the untargeted control *Renilla* luciferase reporter (black bars) as well as the *Firefly* luciferase reporter as a transfection control. HCT-116 cells transfected with only luciferase vectors were also used as MOCK-transfected cells. After performing a dual luciferase assay, the expression levels were normalized to the ratio of the activity of (C) miR-200c-RL and (F) miR-16-RL to that of FL in S-TuD-NC transfected cells and are represented by the mean ± SD (n = 3).

(0.05 nM) into HCT116 cells would not be high. Taken together, these results show that S-TuDs inhibit their target miRNAs at very high efficiencies.

The effects of S-TuD RNA on other family members of the target miRNA

We next tested whether an S-TuD targeting a particular miRNA would exhibit inhibitory effects on other family members of this target molecule, i.e. miRNAs that share the same seed sequence (2–8 bases from the 5′-end). We first investigated the specificity of S-TuD using the miR-200 b/-200 c/-429 family as the target in HCT-116 cells, where the expression of miR-200 c is predominant (Supplementary Figure S6A). We expected that the expression of a reporter containing a sequence that is perfectly complementary to miR-200 c would accurately reflect the functional miR-200 c levels. We tested the inhibitory effects of S-TuD-miR200c-pf and S-TuD-miR429-pf (Figure 6A, B and Supplementary Figure S6B), respectively, and found that the inhibitory activity of S-TuD-miR200c-pf was high, whereas S-TuD-miR429-pf had only slight effects (Figure 6C). These results suggested that strong cross reactivity between miRNA targets is not detectable even when their seed sequences are identical.

Since these observations are somehow different from those obtained for TuD RNA, where significant cross reactivity was detected, we chose the miR-15 a/-15 b/-16/-195/-424/-497 family in HCT-116 cells for analysis as these molecules were previously tested for TuD RNA (19). Since the expression of miR-16 is predominant in HCT-116 cells (Supplementary Figure S6C) the miR-16 reporter mainly reflects the functional levels of this molecule in this experimental setting. We tested the inhibitory effects of S-TuD-miR16-pf, S-TuD-miR195-pf and

S-TuD-miR497-pf, respectively (Figure 6D, E and Supplementary Figure S6D). The inhibitory activity of S-TuD-miR195-pf was equivalent to that of S-TuD-miR16-pf, whereas S-TuD-miR497-pf showed no effects (Figure 6F). These results confirmed that cross-reactivity among target miRNAs requires not only identical seed sequence but also extensive homology between the 3′-compensatory regions (26) of these molecules.

Duration of the inhibitory effects of S-TuD

To confirm that S-TuD can efficiently increase the amount of endogenous proteins targeted by the miRNA, we transfected S-TuD-miR200c-pf or LNA-miR200c into HCT-116 cells and determined the expression levels of the ZEB1 protein which is an established target of miR-200c at 2 days after transfection (28). We observed that S-TuD-miR200c-pf elevated ZEB1 expression compared with S-TuD-NC and further that the elevated level was slightly higher than that of LNA-miR200c (Figure 7A).

Given the high inhibitory effects of S-TuD against its target miRNA, we next analyzed the duration of these effects using S-TuD-miR200c-pf. We first synthesized 5-FAM-labeled S-TuD-miR200c-pf and S-TuD-NC, and confirmed that the 5-FAM label has no impact on the miRNA inhibitory effects of S-TuD (Supplementary Figure S7A). We transfected HCT-116 cells with 5-FAM-labeled S-TuD-miR200c-pf and 5-FAM-labeled S-TuD-NC, respectively, and then sorted 5-FAM-positive cells 2 days later and maintained them in culture (Supplementary Figure S7B–D). In the process of cellular passaging, parallel cultures were prepared for the transfection of *luciferase* reporter genes, the activity of which was assayed 2 days after transfection (Figure 7B). The inhibitory effects of 5-FAM-S-TuD-miR200c-pf were high at 2 days after the introduction of S-TuD and significant inhibitory effects were observed even at 7 days after transfection. The inhibitory effects of 5-FAM-S-TuD-miR200c-pf became marginal by 11 days. We also investigated the duration of the effects on the expression levels of ZEB1. As shown in Figure 7C, the expression levels of ZEB1 were increased at 7 days after S-TuD transfection, but these effects had disappeared at 11 days after transfection, consistent with the reporter assay results. These data indicate that the inhibitory effects of a single transfection of S-TuD are quite long-lasting (>7days) and persist even after several cell divisions (about seven cycles).

An epithelial–mesenchymal transition is induced by miR-200 c inhibition

It has been reported previously that the epithelial–mesenchymal transition (EMT) is induced by inhibiting the activities of the miR-200 family (28). In this previous study, HCT-116 cells were transfected with 50 nM of miRNA inhibitor (LNA) five times every 3 days to establish the EMT. In our current study, we estimated the time required to establish the EMT by suppressing miR-200 family activity via the continuous expression of TuD in HCT-116 cells. We used a lentivirus vector system

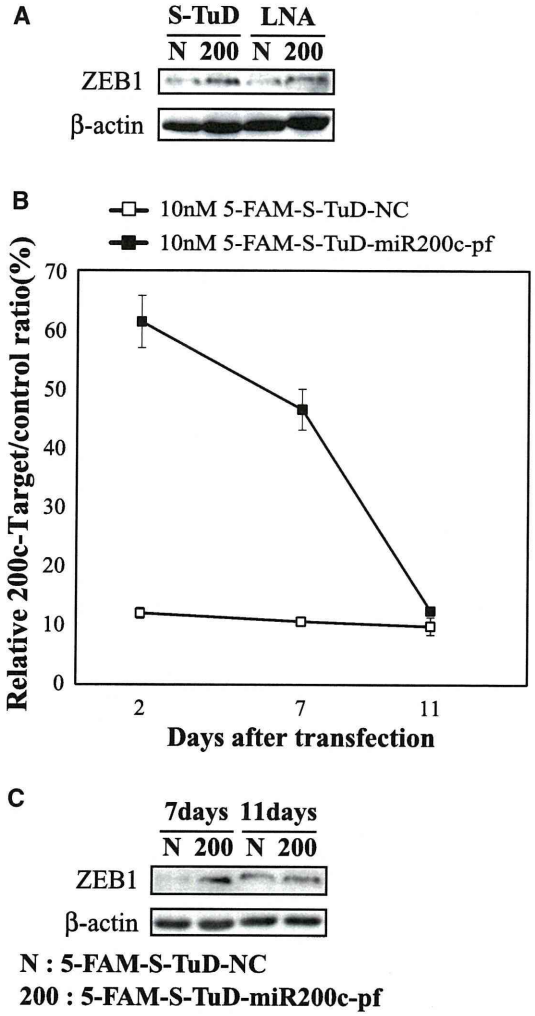

Figure 7. The inhibitory effects of S-TuD-miR200c-pf. (**A**) HCT-116 cells were transfected with S-TuD-miR200c-pf (200), S-TuD-NC (N), LNA-miR200c (200) and LNA-NC (N) at concentrations of 10 nM, respectively. From these transfected cells, total proteins were prepared 2 days after transfection. ZEB1 (top) and β-actin (bottom) were detected by western blotting. (**B**) Time course analysis of the inhibitory effects of S-TuD-miR200c-pf. HCT-116 cells were transfected with 5-FAM labeled S-TuD-miR200c-pf or S-TuD-NC at concentrations of 10 nM and 5-FAM positive cells were flow sorted 2 days after transfection. Sorted cells were maintained in culture and parallel cultures were prepared at each cellular passage for transfection with reporter genes. Dual luciferase assays were performed 2 days after transfection. The relative expression levels were normalized to those of 10 nM 5-FAM-S-TuD-NC transfected HCT-116 cells and are represented by the mean ± SD ($n = 3$). (**C**) The expression levels of ZEB1 in cells shown in (B). Total proteins from these sorted cells were prepared 7 and 11 days after transfection. ZEB1 (top) and β-actin (bottom) were detected by western blotting.

carrying TuD-miR200c expression cassettes driven by the human 7SK promoter which fully inhibited miR-200c in HCT-116 cells (Supplementary Figure S8AB). We next determined the expression levels of E-cadherin and vimentin, as epithelial and mesenchymal markers, respectively, in these cells (Figure 8A). At 7 days after

the transduction of the vector carrying TuD-miR200c, the E-cadherin expression levels were significantly reduced but vimentin expression was only marginally detected. High levels of vimentin expression, concomitant with very low E-cadherin levels, were established by 11 days after TuD-miR200c transduction, indicating that the establishment of EMT requires continuous expression of TuD-miR200c for 8–11 days. In addition, morphological changes into fibroblastic cells were observed and were maintained for at least 1 month (Figure 8B).

Because the inhibitory effects of 5-FAM-S-TuD-miR200c-pf were found to be quite long-lasting and marginal inhibitory effects were detectable even at 11 days after the transfection of HCT-116 cells with this molecule, we evaluated whether EMT could be induced by a single transfection of 5-FAM-S-TuD-miR200c-pf at a 10 nM dose. 5-FAM positive cells were flow sorted and cultured. As shown in Figure 8C, E-cadherin expression was decreased in 5-FAM-S-TuD-miR200c-pf introduced cells at 11 days after transfection, when the larger cellular population assumed a fibroblastic morphology (Figure 8D). However, vimentin induction remained undetectable in these cells. These results indicate that EMT is only partially induced by 5-FAM-S-TuD-miR200c-pf when compared with the full EMT induction observed in HCT-116 cells harboring the TuD-miR200c expression lentivirus vector. Furthermore, the reduction of E-cadherin expression was recovered and this protein

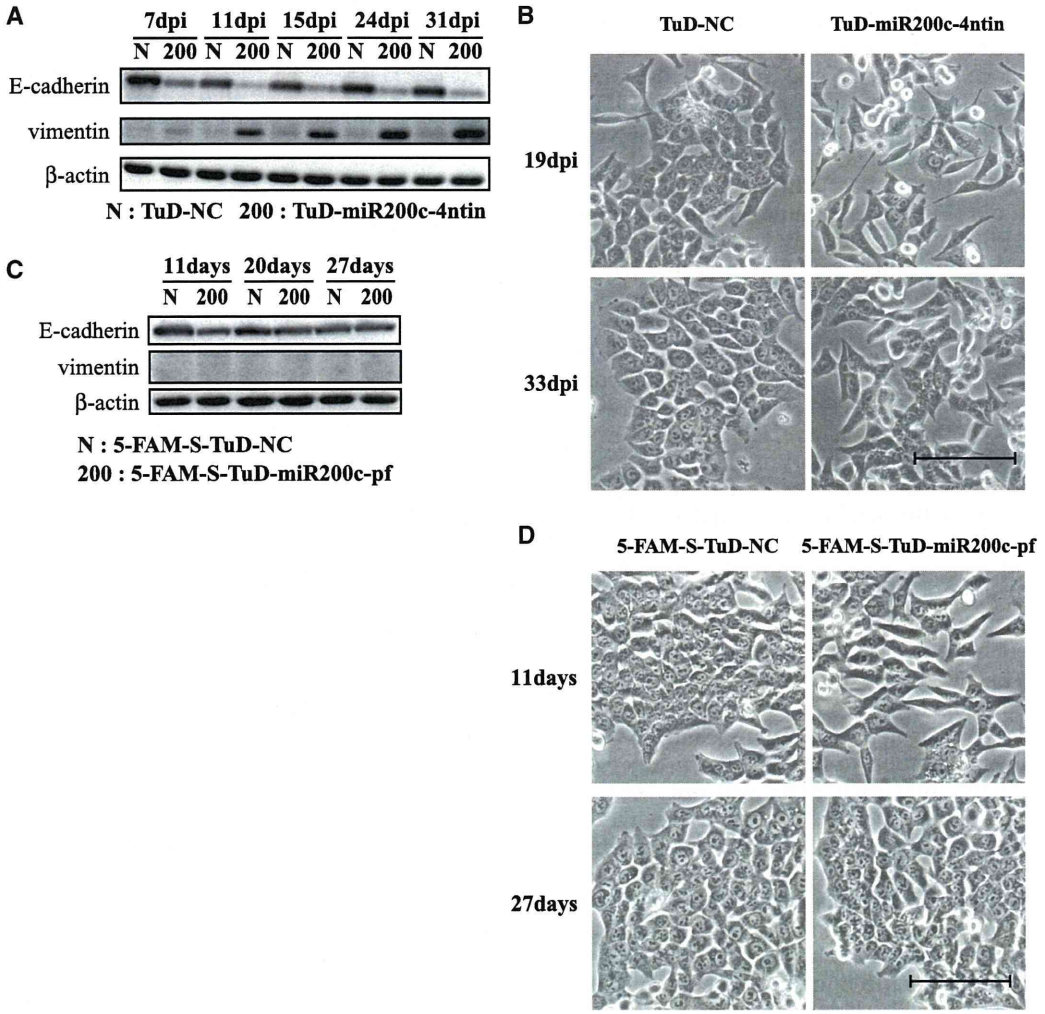

Figure 8. Induction of the EMT by the inhibition of miR-200c. (**A**) A TuD RNA-expressing lentiviral vector was transduced into HCT-116 cells with an MOI of three followed by selection with puromycin. The expression levels of E-cadherin and vimentin, gene markers of the epithelium or mesenchyme, respectively, were then measured. Total proteins were prepared at 7, 11, 15, 24 and 31 days after transduction. E-cadherin (top) and vimentin (middle) and a β-actin loading control (bottom) were detected by western blotting. (**B**) Morphological status of HCT-116 cells transduced with TuD-miR200c-4ntin or TuD-NC expressing lentivirus at 19 and 33 days after transduction. Bar, 10 μm. (**C**) HCT-116 cells were transfected with 5-FAM-S-TuD-miR200c-pf or 5-FAM-S-TuD-NC, both at a concentration of 10 nM, and 5-FAM positive cells were sorted at 2 days after transfection. Total proteins were prepared 11, 20 and 27 days after transfection. E-cadherin (top), vimentin (middle) and β-actin (bottom) were detected by western blotting. (**D**) Morphological status of HCT-116 cells transfected with 5-FAM-S-TuD-miR200c-pf or 5-FAM-S-TuD-NC at 11 and 27 days after transfection. Bar, 10 μm.

reached normal levels at 20–27 days after transfection. At the same time, the fibroblastic morphology of the cells transduced with 5-FAM-S-TuD-miR200c-pf returned fully to the parental epithelial cell appearance (Figure 8D). These results indicate that the E-cadherin reduction and fibroblastic morphology induced by a single transfection of 5-FAM-S-TuD-miR200c-pf is both transient and reversible.

DISCUSSION

In our current study, we have developed a novel synthetic miRNA inhibitor, S-TuD, that has a similar structure to that of TuD RNA, which we previously developed to be expressed from plasmid- or lentivirus vectors (19). Through a single transduction of an optimized S-TuD (S-TuD-miR200c-pf), sufficient miRNA inhibitory effects were obtained and shown to persist for 7 days (about seven cell divisions) and to partially introduce EMT. During the process of optimizing the MBS sequences in our S-TuD design, we found that the two MBS regions within a single S-TuD molecule should not form a threshold level of base pairing, ~9 bp as predicted by CentroidFold (Figure 3 and Supplementary Figure S3). When an MBS that is completely complementary to the target miRNA sequence exceeds this threshold, we found that the introduction of a single mutation or 4 nt insertion in the middle region of the MBS is sufficient in many cases to abolish the base pairing without significantly affecting the affinity to the target miRNA. Although secondary structures composed of 2′-*O*-methylated RNA will differ from those comprising native RNA, we show from our analysis that the secondary structure predictions for three S-TuD-miR21 molecules by CentroidFold were very consistent with the melting curve analysis (Figure 4). Our prediction accuracy, however, will be increased much more if a secondary structure algorithm for 2′-*O*-methylated RNA becomes available.

Our present results show that the inhibitory effects of S-TuD-miR21 were drastically reduced with a stem I length of 10 bp, indicating that S-TuDs requires a long stem I to maintain a rigid structure, where two MBSs are bounded by two stable stems (stem I and II). In such S-TuDs, both ends of the two MBSs are so firmly fixed by the flanking stems that each MBS will not twist freely along with its strand axis. We therefore speculate that this conformational restriction contributes to an efficient access of the MBS to the target miRNA. These unique structural features of S-TuD as well as TuD may explain why S-TuD shows stronger inhibitory activity than other currently available miRNA inhibitors (their basic structural features are summarized in Supplementary Table S2)

In summary, S-TuD shows long-lasting inhibitory effects at very low dosages and has no detectable interferon inducing activity in culture. These characteristics of S-TuD are advantageous for its potential as a future therapeutic drug. Using recent evidence from pharmaceutical research focusing on siRNA, we would like to now develop an efficient drug delivery system for S-TuD and to reduce potential side effects of these molecules, such as unwanted cytokine responses, when they are introduced *in vivo*.

SUPPLEMENTARY DATA

Supplementary Data are available at NAR Online: Supplementary Tables S1–S7. Supplementary Figures S1–S8.

ACKNOWLEDGEMENTS

The authors are grateful to M. Hamada (University of Tokyo and AIST) for kind advice concerning CentroidFold. The authors thank K. Takagi for assistance with the quantitative RT–PCR. The authors also thank the IMSUT FACS Core Laboratory for assistance in using the FACS Aria. Super-computing resources were provided by the Human Genome Center, University of Tokyo, Japan (http://sc.hgc.jp/shirokane.html). The authors are additionally grateful to S. Kawaura and A. Kato for assistance in the preparation of this manuscript.

FUNDING

Grant-in-Aid for Scientific Research on Priority Areas from the Ministry of Education, Culture, Sports, Science and Technology, Japan (MEXT) [17016015]; by a Grant-in-Aid for Young Scientists (B) [22700873]; and by A-Step of the Japan Science and Technology Agency. Funding for open access charge: Grant in AID for Scientific Research on Priority Areas from MEXT.

Conflict of interest statement. None declared.

REFERENCES

1. Ambros,V. (2004) The functions of animal microRNAs. *Nature*, **431**, 350–355.
2. Bartel,D.P. (2004) MicroRNAs: genomics, biogenesis, mechanism, and function. *Cell*, **116**, 281–297.
3. He,L. and Hannon,G.J. (2004) MicroRNAs: small RNAs with a big role in gene regulation. *Nat. Rev. Genet.*, **5**, 522–531.
4. Lin,S.L., Chang,D.C., Chang-Lin,S., Lin,C.H., Wu,D.T., Chen,D.T. and Ying,S.Y. (2008) Mir-302 reprograms human skin cancer cells into a pluripotent ES-cell-like state. *RNA*, **14**, 2115–2124.
5. Li,Q.J., Chau,J., Ebert,P.J., Sylvester,G., Min,H., Liu,G., Braich,R., Manoharan,M., Soutschek,J., Skare,P. *et al.* (2007) miR-181a is an intrinsic modulator of T cell sensitivity and selection. *Cell*, **129**, 147–161.
6. Lu,J., Getz,G., Miska,E.A., Alvarez-Saavedra,E., Lamb,J., Peck,D., Sweet-Cordero,A., Ebert,B.L., Mak,R.H., Ferrando,A.A. *et al.* (2005) MicroRNA expression profiles classify human cancers. *Nature*, **435**, 834–838.
7. Lecellier,C.H., Dunoyer,P., Arar,K., Lehmann-Che,J., Eyquem,S., Himber,C., Saib,A. and Voinnet,O. (2005) A cellular microRNA mediates antiviral defense in human cells. *Science*, **308**, 557–560.
8. Shimono,Y., Zabala,M., Cho,R.W., Lobo,N., Dalerba,P., Qian,D., Diehn,M., Liu,H., Panula,S.P., Chiao,E. *et al.* (2009) Downregulation of miRNA-200c links breast cancer stem cells with normal stem cells. *Cell*, **138**, 592–603.
9. Jopling,C.L., Yi,M., Lancaster,A.M., Lemon,S.M. and Sarnow,P. (2005) Modulation of hepatitis C virus RNA abundance by a liver-specific MicroRNA. *Science*, **309**, 1577–1581.

10. Hutvagner,G., Simard,M.J., Mello,C.C. and Zamore,P.D. (2004) Sequence-specific inhibition of small RNA function. *PLoS Biol.*, **2**, E98.
11. Meister,G., Landthaler,M., Dorsett,Y. and Tuschl,T. (2004) Sequence-specific inhibition of microRNA- and siRNA-induced RNA silencing. *RNA*, **10**, 544–550.
12. Orom,U.A., Kauppinen,S. and Lund,A.H. (2006) LNA-modified oligonucleotides mediate specific inhibition of microRNA function. *Gene*, **372**, 137–141.
13. Davis,S., Lollo,B., Freier,S. and Esau,C. (2006) Improved targeting of miRNA with antisense oligonucleotides. *Nucleic Acids Res.*, **34**, 2294–2304.
14. Krutzfeldt,J., Rajewsky,N., Braich,R., Rajeev,K.G., Tuschl,T., Manoharan,M. and Stoffel,M. (2005) Silencing of microRNAs in vivo with 'antagomirs'. *Nature*, **438**, 685–689.
15. Vermeulen,A., Robertson,B., Dalby,A.B., Marshall,W.S., Karpilow,J., Leake,D., Khvorova,A. and Baskerville,S. (2007) Double-stranded regions are essential design components of potent inhibitors of RISC function. *RNA*, **13**, 723–730.
16. Scherr,M., Venturini,L., Battmer,K., Schaller-Schoenitz,M., Schaefer,D., Dallmann,I., Ganser,A. and Eder,M. (2007) Lentivirus-mediated antagomir expression for specific inhibition of miRNA function. *Nucleic Acids Res.*, **35**, e149.
17. Sayed,D., Rane,S., Lypowy,J., He,M., Chen,I.Y., Vashistha,H., Yan,L., Malhotra,A., Vatner,D. and Abdellatif,M. (2008) MicroRNA-21 targets Sprouty2 and promotes cellular outgrowths. *Mol. Biol. Cell.*, **19**, 3272–3282.
18. Ebert,M.S., Neilson,J.R. and Sharp,P.A. (2007) MicroRNA sponges: competitive inhibitors of small RNAs in mammalian cells. *Nat. Methods*, **4**, 721–726.
19. Haraguchi,T., Ozaki,Y. and Iba,H. (2009) Vectors expressing efficient RNA decoys achieve the long-term suppression of specific microRNA activity in mammalian cells. *Nucleic Acids Res.*, **37**, e43.
20. Sakurai,K., Furukawa,C., Haraguchi,T., Inada,K., Shiogama,K., Tagawa,T., Fujita,S., Ueno,Y., Ogata,A., Ito,M. *et al.* (2011) MicroRNAs miR-199a-5p and -3p target the Brm subunit of SWI/SNF to generate a double-negative feedback loop in a variety of human cancers. *Cancer Res.*, **71**, 1680–1689.
21. Hikichi,M., Kidokoro,M., Haraguchi,T., Iba,H., Shida,H., Tahara,H. and Nakamura,T. (2011) MicroRNA regulation of glycoprotein B5R in oncolytic vaccinia virus reduces viral pathogenicity without impairing its antitumor efficacy. *Mol. Ther*, **19**, 1107–1115.
22. Lu,Z., Li,Y., Takwi,A., Li,B., Zhang,J., Conklin,D.J., Young,K.H. and Martin,R. (2011) miR-301a as an NF-κB activator in pancreatic cancer cells. *EMBO J.*, **30**, 57–67.
23. Gagan,J., Dey,B.K., Layer,R., Yan,Z. and Dutta,A. (2011) MicroRNA-378 targets the myogenic repressor MyoR during myoblast differentiation. *J. Biol. Chem.*, **286**, 19431–19438.
24. Elbashir,S.M., Lendeckel,W. and Tuschl,T. (2001) RNA interference is mediated by 21- and 22-nucleotide RNAs. *Genes Dev.*, **15**, 188–200.
25. Sato,K., Hamada,M., Asai,K. and Mituyama,T. (2009) CENTROIDFOLD: a web server for RNA secondary structure prediction. *Nucleic Acids Res.*, **37**, W277–W280.
26. Brennecke,J., Stark,A., Russell,R.B. and Cohen,S.M. (2005) Principles of microRNA-target recognition. *PLoS Biol.*, **3**, e85.
27. Zeng,Y. and Cullen,B.R. (2004) Structural requirements for pre-microRNA binding and nuclear export by Exportin 5. *Nucleic Acids Res.*, **32**, 4776–4785.
28. Park,S.M., Gaur,A.B., Lengyel,E. and Peter,M.E. (2008) The miR-200 family determines the epithelial phenotype of cancer cells by targeting the E-cadherin repressors ZEB1 and ZEB2. *Genes Dev.*, **22**, 894–907.

THE JOURNAL OF BIOLOGICAL CHEMISTRY VOL. 287, NO. 15, pp. 11924–11933, April 6, 2012

Double Plant Homeodomain (PHD) Finger Proteins DPF3a and -3b Are Required as Transcriptional Co-activators in SWI/SNF Complex-dependent Activation of NF-κB RelA/p50 Heterodimer*[S]

Received for publication, November 10, 2011, and in revised form, January 30, 2012 Published, JBC Papers in Press, February 13, 2012, DOI 10.1074/jbc.M111.322792

Aya Ishizaka[‡1], Taketoshi Mizutani[‡§], Kazuyoshi Kobayashi[‡], Toshio Tando[‡], Kouhei Sakurai[‡], Toshinobu Fujiwara[¶], and Hideo Iba[‡2]

From the [‡]Division of Host-Parasite Interaction, Department of Microbiology and Immunology, Institute of Medical Science, University of Tokyo, 4-6-1 Shirokanedai, Minato-ku, Tokyo 108-8639, [§]RNA and Biofunctions, PRESTO, Japan Science and Technology Agency, 4-1-8 Honcho, Kawaguchi, Saitama 332-0012, and the [¶]Institute of Microbial Chemistry Laboratory of Disease Biology, 3-14-23 Kamiosaki, Shinagawa-ku, Tokyo 141-0021, Japan

Background: The NF-κB dimer, RelA/p50, often requires the SWI/SNF complex for its transactivation function, but its molecular mechanisms remain elusive.
Results: The NF-κB canonical pathway induced by TNF-α is DPF3a/b- and SWI/SNF-dependent for some promoters.
Conclusion: DPF3a and DPF3b are effective linkers for the SWI/SNF complex and RelA/p50.
Significance: The NF-κB·DPF3a/b·SWI/SNF complex would be an effective platform for promoter-specific transactivation.

We have previously shown that DPF2 (requiem/REQ) functions as a linker protein between the SWI/SNF complex and RelB/p52 NF-κB heterodimer and plays important roles in NF-κB transactivation via its noncanonical pathway. Using sensitive 293FT reporter cell clones that had integrated a SWI/SNF-dependent NF-κB reporter gene, we find in this study that the overexpression of DPF1, DPF2, DPF3a, DPF3b, and PHF10 significantly potentiates the transactivating activity of typical NF-κB dimers. Knockdown analysis using 293FT reporter cells that endogenously express these five proteins at low levels clearly showed that DPF3a and DPF3b, which are produced from the *DPF3* gene by alternative splicing, are the most critical for the RelA/p50 NF-κB heterodimer transactivation induced by TNF-α stimulation. Our data further show that this transactivation requires the SWI/SNF complex. DPF3a and DPF3b are additionally shown to interact directly with RelA, p50, and several subunits of the SWI/SNF complex *in vitro* and to be co-immunoprecipitated with RelA/p50 and the SWI/SNF complex from the nuclear fractions of cells treated with TNF-α. In ChIP experiments, we further found that endogenous DPF3a/b and the SWI/SNF complex are continuously present on HIV-1 LTR, whereas the kinetics of RelA/p50 recruitment after TNF-α treatment correlate well with the viral transcriptional activation levels. Additionally, re-ChIP experiments showed DPF3a/b and the SWI/SNF complex associate with RelA on the endogenous *IL-6* promoter after TNF-α treatment. In conclusion, our present data indicate that by linking RelA/p50 to the SWI/SNF complex, DPF3a/b induces the transactivation of NF-κB target gene promoters in relatively inactive chromatin contexts.

NF-κB[3] is a key transcription factor that regulates many biological processes, such as immune, inflammatory, and virus responses, development, cellular growth, and apoptosis. The regulation by NF-κB is achieved through the transactivation of a large number of its target genes in a cell type-specific and/or stimulus-specific manner (1–4). NF-κB is itself composed of homo- or heterodimeric complexes of members of the NF-κB family of proteins, which include RelA (p65), RelB, c-Rel, p50, and p52 in humans. NF-κB dimers remain inactive in the cytoplasm until specific stimulation activates their signaling pathways (5). One of the main NF-κB pathways, the canonical pathway, is triggered by stimulation with factors such as tumor necrosis factor-α (TNF-α) and lipopolysaccharide (LPS). The induction of this pathway results in the activation of the RelA/p50 heterodimer by transporting it to the nucleus after phosphorylation and also the proteasomal degradation of inhibitor of NF-κB (IκB), which retains RelA/p50 in the cytoplasm under unstimulated conditions (6). However, RelB/p52, which is present in the cytoplasm as inactive RelB/p100 (NF-κB1) until stimulated, is activated through the noncanonical pathway (7). This pathway is triggered by stimuli such as lymphotoxin exposure, and it induces the cleavage of cytosolic p100 to produce p52, which subsequently translocates into the nucleus as a RelB/p52 dimer.

* This work was supported by Grants-in-aid for Scientific Research on Priority Areas 17016015 and for Scientific Research (B) 22300318 and (C) 21590507 from the Ministry of Education, Culture, Sports, Science and Technology, Japan, and by a grant from the Japan Society for the Promotion of Science.
[S] This article contains supplemental Figs. S1-S9, Table S1, and experimental procedures.
[1] Research Fellow of the Japan Society for the Promotion of Science.
[2] To whom correspondence should be addressed: Division of Host-Parasite Interaction, Dept. of Microbiology and Immunology, Institute of Medical Science, University of Tokyo, 4-6-1 Shirokanedai, Minato-ku, Tokyo 108-8639, Japan. Tel.: 81-3-5449-5730; Fax: 81-3-5449-5449; E-mail: iba@ims.u-tokyo.ac.jp.

[3] The abbreviations used are: NF-κB, nuclear factor-κB; PHD, plant homeodomain; Luc, luciferase.

The mechanism by which each NF-κB dimer is recruited to a certain set of promoters and specifically transactivates their transcription in a cell type-dependent manner is an important question. Such processes would likely involve chromatin context-dependent regulation. Indeed, NF-κB transactivation is known to often require the SWI/SNF complex, a representative chromatin remodeling factor involved in epigenetic regulation in humans, but no clear and direct interaction between NF-κB components and the SWI/SNF complex has been reported. The SWI/SNF complex has two alternative ATPases, Brahma (Brm) or Brahma-related gene 1 (BRG1) as the catalytic subunits, and other subunits such as BAF155, Ini1/SNF5, BAF170, BAF60a, and β-actin (8–10). The SWI/SNF complex is recruited to target genes via association with transcription regulators such as c-Myc (11), C/EBPβ (12), AP-1 (13), neuron-restrictive silencer factor (14), and Cdx2 (15). In addition to cellular targets, we have shown that integrated LTRs of murine leukemia virus (16, 17) and HIV-1 (human immunodeficiency virus-1) (18) require the Brm-type SWI/SNF complex to maintain their gene expression.

We have recently shown that DPF2 (REQ/BAF45d) functions as an efficient adaptor protein between the SWI/SNF complex and RelB/p52 and plays important roles in NF-κB transcriptional activation at the most downstream part of the NF-κB noncanonical pathway (19). DPF2 belongs to the d4 family of proteins, the members of which are characterized by an N-terminal 2/3 domain containing a nuclear localization signal, a central C2H2-type Krüppel-like zinc finger motif, and a C-terminal d4 domain consisting of a tandem repeat of the PHD zinc finger (20–22). It was previously shown that another member of the d4 family, DPF3 (Cerd4/BAF45c), associates with the SWI/SNF complex and further that the *DPF3* gene has two splicing variants, the products of which differ at their C-terminal regions. The DPF3b protein shows all of the characteristics of a d4 family member, including binding activity to either methylated or acetylated lysine residues at histones H3 and H4 through the PHD fingers. However, DPF3a lacks these binding activities as it harbors a truncated d4 domain within its first PHD (23). Interestingly, two d4 family members, DPF1 (Neud4/BAF45b) and DPF3, and an additional protein, PHF10 (BAF45a), which also possesses double PHD fingers within its C terminus, have been reported to associate with the SWI/SNF complex in neural cells in a differentiation-specific manner (24). In mouse neural progenitors, the complex contains PHF10, but this component is substituted by DPF1 or DPF3 when the cells become differentiated into post-mitotic neurons.

Considering our previous finding that DPF2 is required for RelB/p52 transactivation via the SWI/SNF complex, we speculate that the five proteins DPF1, DPF2, DPF3a, DPF3b, and PHF10 are candidate co-activators of the typical NF-κB heterodimer, RelA/p50, as well as two other NF-κB dimers, RelB/p52 and c-Rel/p50. We show in our current analysis that each of these proteins can enhance the different NF-κB heterodimers to transactivate their targets efficiently when both they and the NF-κB components are exogenously expressed. We further show from our analysis that among these five proteins DPF3a and DPF3b are the most effective cofactors for RelA/p50 activation in 293FT cells treated with TNF-α. Our current data further indicate that these two proteins directly bind to RelA, p50, and at least four subunits of the SWI/SNF complex *in vitro*. We additionally show that endogenous DPF3a/b and the SWI/SNF complex are continuously co-localized at the HIV-1 LTR throughout the period of TNF-α stimulation and that RelA/p50 is promptly recruited to the typical NF-κB-binding sites within the HIV-1 LTR or endogenous *IL-6* promoter upon stimulation. Finally, we show that the viral transcripts are synthesized with similar kinetics to those of RelA/p50 recruitment.

EXPERIMENTAL PROCEDURES

Cell Culture and Retro- and Lentiviral Vectors—293FT cells (Invitrogen) were maintained in Dulbecco's modified Eagle's medium (Wako Chemicals, Tokyo) containing 10% fetal calf serum at 37 °C and 5% CO_2. For TNF-α stimulation, the cells were treated with 10 ng/ml TNF-α (R&D Systems, Minneapolis, MN). Vesicular stomatitis virus G protein (VSV-G)-pseudotyped retro- or lentiviral vectors were prepared as described previously (17, 19). For transduction, cells were incubated with the virus vector stocks in the presence of 8 μg/ml Sequabrene™ (Sigma).

Antibodies—Rabbit polyclonal antibodies against human DPF3 were raised against a synthetic peptide corresponding to amino acid residues 230–251 of the protein (NP_036206) by Medical and Biological Laboratories (MBL, Nagoya, Japan). Other antibodies used in this research are as follows: normal rabbit IgG (PM035) (MBL), α-RelA (C-20), α-BRG-1 (H-88), α-BAF155 (H-76) (Santa Cruz Biotechnology, Santa Cruz, CA), α-p105/p50 (ab7971), α-Brm (ab15597) (Abcam, Cambridge, MA), α-FLAG (M2) (Sigma), α-BAF60a (611728), and α-Ini1 (612110) (BD Transduction Laboratories, San Jose, CA). Most of these specific antibodies are rabbit polyclonal, except α-FLAG, α-BAF60a, and α-Ini1 which are mouse monoclonal.

GST Fusion Protein Pulldown Assays—GST fusion proteins were expressed in *Escherichia coli* Rosetta 2 (Novagen, Madison, WI) via incubation of the cells with 0.1 mM isopropyl 1-thio-β-D-galactopyranoside overnight at 15 °C and then prepared using His tag Binding/Wash Buffer (20 mM Tris-HCl (pH 8.0), 600 mM NaCl, 1 mM $MgCl_2$, 10% glycerol, 0.1% Nonidet P-40, 20 mM imidazole, and phosphatase inhibitors). Purification of GST-His-tagged proteins was performed sequentially using Profinity IMAC nickel-charged resin (Bio-Rad) and glutathione-Sepharose 4B (GE Healthcare). The target proteins were eluted from these columns with His tag Elution Buffer (20 mM Tris-HCl (pH 8.0), 600 mM NaCl, 1 mM $MgCl_2$, 10% glycerol, 0.1% Nonidet P-40, 250 mM imidazole, and phosphatase inhibitors) and GST Elution Buffer (100 mM Tris-HCl (pH 8.0), 12 mM NaCl, 20 mM glutathione, and phosphatase inhibitors), respectively. *In vitro* transcription and translation were then performed as described previously (19). *In vitro* synthesized proteins were incubated with respective GST fusion proteins for 2 h at 4 °C on a rotating platform. The complexes were washed for five times with TNE buffer (10 mM Tris-HCl (pH 7.8), 150 mM NaCl, 1 mM EDTA, 1% Nonidet P-40, and protease inhibitors) and analyzed by SDS-PAGE followed by autoradiography using FLA-5100 (Fujifilm). Cellular lysates, prepared in TN buffer (10 mM Tris-HCl (pH 7.8), 150 mM NaCl, 1% Nonidet P-40, protease inhibitors, and phosphatase inhibitors) were

treated with 100 units/ml benzonase endonuclease (Novagen) and precleared by incubation with GST protein immobilized on beads for 1 h. The lysate was then incubated with respective GST fusion proteins for 4 h at 4 °C on a rotating platform. The complexes were subsequently washed three times with Buffer D (20 mM HEPES-KOH (pH 7.9), 20% glycerol, 0.1 M KCl, 0.2 mM EDTA, 0.1% Nonidet P-40, and protease inhibitors) and analyzed by immunoblotting.

Chromatin Immunoprecipitation (ChIP) and Sequential ChIP Assays—Cells were cross-linked with 1% formaldehyde at 37 °C for 8 min. Cross-linking reactions were stopped by the addition of a 0.1 volume of 1.5 M glycine and incubation at room temperature for 5 min. The cells were then washed with PBS, collected, and incubated in lysis buffer 1 (50 mM HEPES (pH 7.5), 140 mM NaCl, 1 mM EDTA, 10% glycerol, 0.5% Nonidet P-40, 0.25% Triton X-100, and protease inhibitors). Cell lysates were sequentially replaced with lysis buffer 2 (10 mM Tris-HCl (pH 8.0), 200 mM NaCl, 1 mM EDTA, 0.5 mM EGTA, and protease inhibitors), and lysis buffer 3 (10 mM Tris-HCl (pH 8.0), 300 mM NaCl, 1 mM EDTA, 0.5 mM EGTA, 0.1% sodium deoxycholate, 0.5% *N*-lauroylsarcosine, and protease inhibitors). The lysates were then sonicated using Elestein Ryuseikai (Elekon Science. Corp., Chiba, Japan) on ice so that the DNA would be sheared into small fragments with an average length of less than 0.5 kb. After the addition of a 0.1 volume of 10% Triton X-100, the lysates were centrifuged to remove cellular debris and incubated overnight on a rotating platform at 4 °C with the respective antibodies (10 μg of each), which were previously bound to Dynabeads protein G (Invitrogen). The beads were washed once in low salt buffer (20 mM Tris-HCl (pH 8.0), 150 mM NaCl, 2 mM EDTA, 0.1% SDS, 1% Triton X-100, and protease inhibitors), twice in high salt buffer (20 mM Tris-HCl (pH 8.0), 400 mM NaCl, 2 mM EDTA, 0.1% SDS, 1% Triton X-100, and protease inhibitors), five times in RIPA buffer (50 mM HEPES (pH 7.6), 500 mM LiCl, 1 mM EDTA, 0.1% SDS, 1% Triton X-100, and protease inhibitors), and once in a TE, 50 mM NaCl buffer. The immune complexes were harvested in elution buffer (10 mM Tris-HCl (pH 7.5), 1 mM EDTA, 1% SDS and 100 mM DTT). For re-ChIP assays, the eluted complexes were diluted 1:10 with dilution buffer (10 mM Tris-HCl (pH 7.5), 150 mM NaCl, 1 mM EDTA, 0.5% sodium deoxycholate, 1% Nonidet P-40, and protease inhibitors), and the steps of ChIP assay were repeated. Cross-linking was reversed by incubation overnight at 65 °C with a 0.04 volume of 5 M NaCl. After treatment with proteinase K (Wako), the DNA was purified using Nucleospin Extract II (Macherey-Nagel, Düren, Germany) and quantified by real time PCR on a 7300 Real Time PCR System (Applied Biosystems, Bedford, MA) using Premix Ex Taq (Probe qPCR) or SYBR Premix Ex Taq (Takara Bio, Shiga, Japan). The specific primer pairs and probes used in this study are listed in supplemental Table S1.

Other Procedures—Details of the materials and methods used in this study can be found in the supplemental experimental procedures.

RESULTS

High Expression of Each Member of the d4 Family and PHF10 Enhances the Transactivating Activity of RelA/p50, RelB/p52, and c-Rel/p50—We previously generated a 293FT cell line stably harboring an exogenous expression unit composed of tandem NF-κB-responsive elements, a minimum promoter (MinP), and the downstream luciferase (Luc) reporter gene (293FT-NF-κB-MinP-Luc) (Fig. 1*A*) (Ref 19), in which the NF-κB-binding sites were derived from HIV-1 LTR (Fig. 1*B*). Whereas this reporter cell system was useful in evaluating chromosome structure-dependent NF-κB transactivation, it was found not to be as sensitive in responding to the exogenous introduction of NF-κB. We thus isolated several additional cellular clones from this parental reporter cell population and tested each for Luc inducibility following TNF-α treatment. A clone, which we designated as 293FT-NF-κB-MinP-Luc-A3, (abbreviated as NF-κB-MinP-Luc-A3 hereafter), showed one of the highest levels of Luc inducibility by TNF-α and was selected for further analysis (supplemental Fig. S1).

Expression vectors for the five co-activator candidate proteins, four d4 family proteins and PHF10 (supplemental Fig. S2), as well as the empty vector (CV-1) as a control were transfected into NF-κB-MinP-Luc-A3 together with each pair of plasmids expressing the NF-κB dimer, RelA/p50, RelB/p52, or c-Rel/p50, as well as the control vector for NF-κB expression (CV-2). The expression of these five candidate proteins that were tagged with FLAG at their N termini were confirmed by immunoblotting (supplemental Fig. S3*A*). As shown in Fig. 1*C*, the basal Luc activity in cells transfected with CV-2 was not significantly affected by the introduction of any of the candidate proteins (*lanes 2–6* compared with *lane 1*). Compared with the Luc activity of cells transfected with CV-1, the introduction of RelA/p50, RelB/p52, and c-Rel/p50 increased these reporter expression levels by 42-, 6-, and 3-fold, respectively (Fig. 1*C*, *lanes 13, 19,* and *7* compared with *lane 1*). These results indicated that NF-κB-MinP-Luc-A3 has very low basal NF-κB activity and that none of the candidates have any effects alone under these conditions, even if expressed at high levels. Importantly, transactivation mediated through RelA/p50 (Fig. 1*C*, *lanes 14–18* compared with *lane 13*), RelB/p52 (*lanes 20–24* compared with *lane 19*), and c-Rel/p50 (*lanes 8–12* compared with *lane 7*) was enhanced by the endogenous expression of any of the five candidate proteins (*lanes 7–24*). No significant differences were found among these five proteins in terms of the enhancement of any of the three NF-κB dimers, suggesting that all potentially function as co-activators of NF-κB in any context, at least when expressed at high levels.

Both DPF3a and DPF3b Are Required for SWI/SNF-dependent Transcriptional Activation through the NF-κB Canonical Pathway—We concluded that transfection experiments involving NF-κB expression vectors would not fully reflect NF-κB activation induced by naturally occurring signal transduction pathways and that the transient expression of candidate proteins by plasmid vectors is very high and thus far from physiological (supplemental Fig. S4). Hence, the experimental conditions used above would most likely not reflect the functional specificity of these proteins correctly. We thus examined the requirement for each candidate protein in the activation of NF-κB by TNF-α treatment, which strongly and almost exclusively activates the endogenous RelA/p50 dimer. Because 293FT cells express all of the transcripts coding these five can-

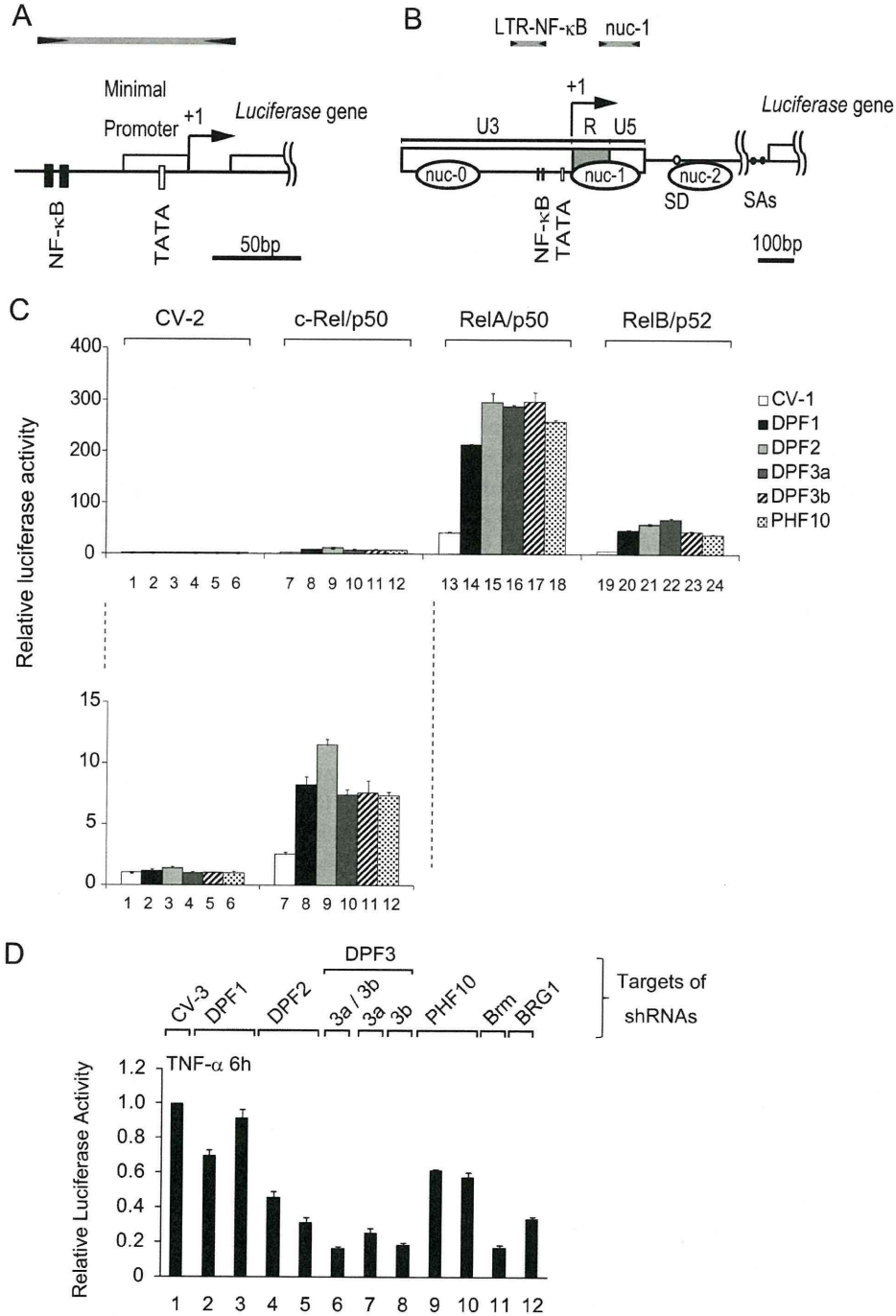

FIGURE 1. **d4 family members are potentially involved in both the canonical and noncanonical NF-κB transactivation of SWI/SNF-dependent promoters.** *A* and *B*, schematic representation of the constructs used in this study: NF-κB-MinP (*A*) and HIV-1 LTR (*B*). The binding sites for NF-κB and the TATA boxes are highlighted by *black* and *white bars*, respectively. Transcriptional start sites are designated as +1. Positions detected by real time PCR are indicated by *black arrows* and *gray bars*. The splicing donor and the acceptors are indicated by *white* and *black circles*. *C*, NF-κB-MinP-Luc-A3 cells were cotransfected with 10 ng of vectors expressing NF-κB subunits and 490 ng of candidate protein expressing or respective control vectors in different combinations. Luciferase activity was measured 48 h after transfection and normalization using control plasmid transfectants. *D*, NF-κB-MinP-Luc-A3 cells were transfected with 500 ng of vectors expressing short hairpin RNAs against each candidate protein and also *Brm* or *BRG1*. At 42 h post-transfection, cells were treated with 10 ng/ml TNF-α for 6 h, which led to a 1500-fold activation of luciferase activity compared with the control vector (CV-3) transfectants (data not shown). Luciferase activities were normalized to the CV-3 control transfectants. The corresponding target sites of the shRNAs against each of the candidates analyzed in this experiment are shown in supplemental Fig. S1. *Lane 2*, shDPF1-cds-1; *lane 3*, shDPF1-utr-1; *lane 4*, shREQ#1; *lane 5*, shREQ#2; *lane 6*, shDPF3-cds-1; *lane 7*, shDPF3a-utr-2; *lane 8*, shDPF3b-cds-3; *lane 9*, shPHF10-cds-1; and *lane 10*, shPHF10-utr-1. The results presented here are the average of at least three independent experiments, and the *bars* indicate the standard deviation.

didate proteins, as judged by semi-quantitative RT-PCR (supplemental Fig. S3*B* and data not shown), we performed knockdown experiments using the same assay cell line, NF-κB-MinP-Luc-A3. The efficiency and specificity of each of the designed shRNAs were confirmed by semi-quantitative RT-PCR or immunoblotting using 293FT cells (supplemental Fig. S3, *B* and

C). The NF-κB-MinP-Luc-A3 cell line was transfected with a vector that expresses shRNA targeting each candidate protein and the catalytic subunits of the SWI/SNF complex as well as a control shRNA vector (CV-3). At 42 h after transfection, cultures were treated with or without TNF-α for an additional 6 h.

Upon TNF-α stimulation, Luc activity increased by 1400-fold when the cells were transfected with CV-3. The knockdown of Brm and BRG1, the alternative catalytic subunits of the SWI/SNF complex, caused a significant reduction in transactivation by 82 and 66%, respectively (Fig. 1*D, lanes 11* and *12*), indicating that NF-κB-MinP in the reporter cell line requires the SWI/SNF complex to be activated through the NF-κB canonical pathway. The depletion of DPF2 (Fig. 1*D, lanes 4* and *5*) and PHF-10 (Fig. 1*D, lanes 9* and *10*) lowered the ability of TNF-α to activate this promoter by 60 and 40% respectively, and the knockdown of DPF1 (Fig. 1*D, lanes 2* and *3*) marginally but clearly reduced the Luc promoter activity. These results are consistent with the notion deriving from the results of the overexpression experiments (Fig. 1*C*) that DPF1, DPF2, and PHF10 contribute to transactivation via the endogenous RelA/p50 dimer and the difference among the effects of each knockdown might be somehow reflecting their endogenous levels. Interestingly, the simultaneous depletion of DPF3a and DPF3b by a single shRNA, whose targeting site is within the shared region for these proteins, was shown to reduce TNF-α-dependent activation by 84% (Fig. 1*D, lane 6*). Furthermore, a single knockdown of either DPF3a or DPF3b also caused a comparative reduction in promoter activation (Fig. 1*D, lanes 7* and *8*). These results suggest that in these cells, among the tested candidates, either DPF3a or DPF3b have the most crucial role in the canonical NF-κB pathway, which cannot be efficiently compensated for by the other candidate proteins. The overall results shown in Fig. 1*D* were almost identically obtained using another 293FT clone K5 (supplemental Fig. S5). Taken together, these data support the idea that in 293FT cells DPF3a and DPF3b are the most critical factors required for RelA/p50 to activate this NF-κB-containing promoters in an SWI/SNF-dependent manner, and we therefore decided to further concentrate our analysis on DPF3a and DPF3b.

Both DPF3a and DPF3b Directly Bind to RelA and p50 as Well as Several Subunits of the SWI/SNF Complex in Vitro—Because DPF3a and DPF3b were found to be required for SWI/SNF complex-dependent RelA/p50 transactivation, we next evaluated the proteins with which DPF3a and DPF3b can associate *in vitro*. We first performed glutathione *S*-transferase pulldown assays using purified GST alone, GST-DPF3a, and -DPF3b and several subunits of the SWI/SNF complex translated *in vitro* in the presence of [^{35}S]methionine (supplemental Fig. S6). Both DPF3a and DPF3b directly bound to Brm, BRG1, Ini1, and BAF60a but not to β-actin, which are similar binding properties to those of DPF2 that we have previously reported (19).

We next performed a similar assay using *in vitro* translated RelA and p50 and GST-fused DPF3a and DPF3b as well as DPF2. As shown in Fig. 2*A*, either RelA or p50 alone as well as in combination with both proteins synthesized in the same translating mixture were found to directly associate with DPF3a and DPF3b. We also found that RelA or p50 alone also binds to DPF2 to a lesser extent. These binding properties of DPF2 are fully consistent with our previous report (19). In the current experiments, these two GST proteins were tagged with His_6 at their C termini to enable higher purification and the performance of a more sensitive binding assay (supplemental Fig. S7). We performed further GST pulldown assays using the same purified GST proteins and 293FT whole cell extracts obtained from cells stimulated with or without TNF-α as the input proteins. The extracts were treated with benzonase endonuclease to avoid detecting interactions mediated through DNA or RNA fragments. The pulled down cellular proteins were analyzed by immunoblotting, and as shown in Fig. 2*B*, both DPF3a and DPF3b were found to associate with endogenous RelA and BRG1. Importantly, the binding affinities for DPF3a and DPF3b in these cases were not significantly increased by TNF-α stimulation. It should be pointed out here that in the total protein preparations subcellular localization of natural NF-κB is disrupted. These results therefore suggest that the binding potential of RelA to DPF3a and DPF3b is not significantly enhanced by post-translational modifications of RelA triggered by TNF-α stimulation (25–28). Taken together, our findings indicate that both DPF3a and DPF3b have the potential to directly associate with RelA/p50 and the SWI/SNF complex and further that the binding potential is not enhanced by post-translational modifications of NF-κB or the SWI/SNF complex triggered by TNF-α.

DPF3 Interacts with the SWI/SNF Complexes and RelA/p50 in the Nucleus—We prepared 293FT cells stably expressing either FLAG-tagged DPF3a or DPF3b through the introduction of retrovirus vectors (293FT-FLAG-DPF3a and 293FT-FLAG-DPF3b) and isolated nuclear fractions from each cell type with or without TNF-α treatment. We then performed a co-immunoprecipitation assay using α-FLAG antibodies (Fig. 2*C*). The subunits of the SWI/SNF complex, Brm, BRG1, and BAF155, were found to be co-immunoprecipitated with either DPF3a or DPF3b, independently of TNF-α stimulation. In the immunoprecipitates with FLAG-DPF3b, both RelA and p50 were detected specifically in TNF-α-stimulated cells, indicating that DPF3b efficiently associates with both RelA and p50, which are recruited to the nucleus. In the immunoprecipitates with FLAG-DPF3a from TNF-α-stimulated cells, p50 was detected, whereas only marginal levels of RelA were detectable, suggesting that DPF3a binds RelA/p50 at a lower affinity than DPF3b in the nucleus. Our observations therefore suggest that the association between DPF3a/b and RelA/p50 occurs following RelA/p50 translocation to the nucleus where DPF3a or -3b consistently interacts with the SWI/SNF complex. When similar analyses were performed on the other candidate proteins, DPF1 and DPF2 showed similar binding properties to DPF3a and -3b for the associations with the SWI/SNF complex and RelA/p50 (supplemental Fig. S8).

To further analyze the DPF3 interaction with the RelA/p50 and SWI/SNF complex, we prepared whole cell extracts from 293FT-FLAG-DPF3a and 293FT-FLAG-DPF3b with or without TNF-α treatment (Fig. 2*D*). Each cellular extract was again treated with benzonase endonuclease and then subjected to a co-immunoprecipitation assay using α-FLAG antibodies. Brm, BRG1, BAF155, and BAF60a were all successfully co-immunoprecipitated from the total cellular lysates of both 293FT-

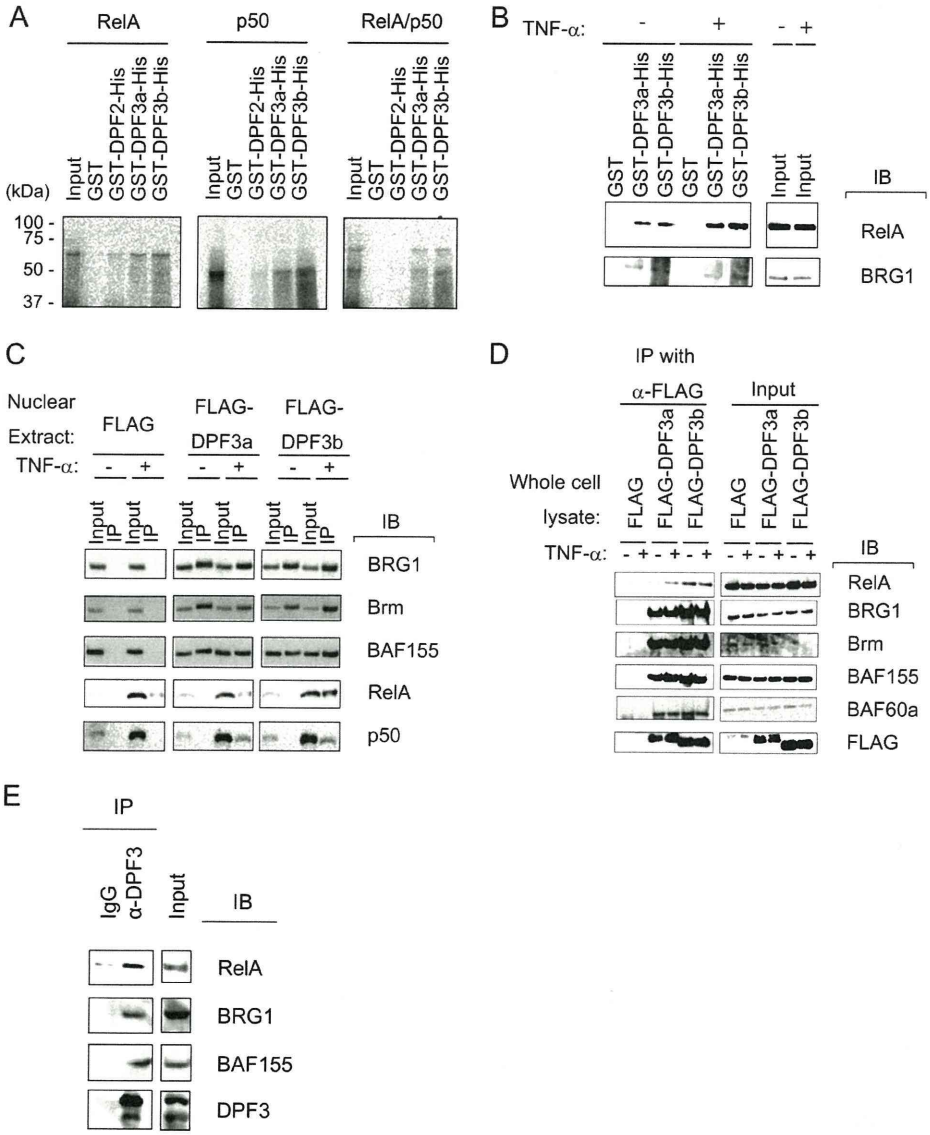

FIGURE 2. **DPF3a and -3b associate with both RelA/p50 and the SWI/SNF complex.** *A*, [^{35}S]methionine-labeled RelA and p50 were translated using a wheat germ extract system *in vitro* and incubated with GST alone and GST-His-tagged DPF2, DPF3a, or DPF3b. These interactions were analyzed by SDS-PAGE followed by autoradiography. *B*, 293FT cells were stimulated with or without 10 ng/ml TNF-α for 10 min, and whole cell lysates were then obtained and subjected to benzonase endonuclease treatment. The lysate was incubated with GST alone, GST-His-tagged DPF2, DPF3a, or DPF3b, and pulled down materials were analyzed by immunoblotting. *C*, 293FT cells were stimulated with or without 10 ng/ml TNF-α for 10 min, and whole cell lysates were obtained and treated with endonuclease. Immunoprecipitation (*IP*) assays were performed using α-FLAG antibodies, and precipitated materials were eluted with free FLAG peptide and analyzed by immunoblotting (*IB*). *D*, 293FT cells stably expressing FLAG, FLAG-DPF3a, or FLAG-DPF3b were stimulated with or without 10 ng/ml TNF-α for 60 min. Nuclear extracts were then prepared and subjected to immunoprecipitation assays with α-FLAG antibodies followed by immunoblotting. *E*, 293FT cells were treated with 10 ng/ml TNF-α for 20 min, and whole cell lysate was obtained and treated with endonuclease. Immunoprecipitation assays were performed using α-DPF3 antibody, and precipitated materials were analyzed by immunoblotting.

FLAG-DPF3a and -DPF3b independently of TNF-α. RelA was found to be co-immunoprecipitated with DPF3b and to a lesser extent with DPF3a. DPF3a and DPF3b would associate with RelA after the preparation of the whole cell extracts from unstimulated cells, where the natural NF-κB subcellular localizations are disrupted. These data again support that the RelA binding potential to DPF3a or DPF3b was not significantly affected by TNF-α treatment, consistent with the results shown in Fig. 2*B*.

To finally show our observations that DPF3a/b associates with RelA/p50 or the SWI/SNF complex is valid even in non-manipulated cells, we treated 293FT cells with TNF-α for 20 min and immunoprecipitated endogenous DPF3a and DPF3b with antibody against DPF3, which does not discriminate between DPF3a and DPF3b. The immunoprecipitates were analyzed, and endogenous DPF3a/b was shown to associate with RelA, BRG1, and BAF155, just like exogenously introduced DPF3 proteins (Fig. 2*E*).

Kinetics of RelA Recruitment upon TNF-α Stimulation Correlate with Those of Primary Transcript Production from Both Artificial and Natural Promoters—To understand molecular mechanisms involved in transcriptional activation after TNF-α stimulation, we next analyzed the kinetics of RelA recruitment and transactivation. Following cellular exposure to TNF-α, it

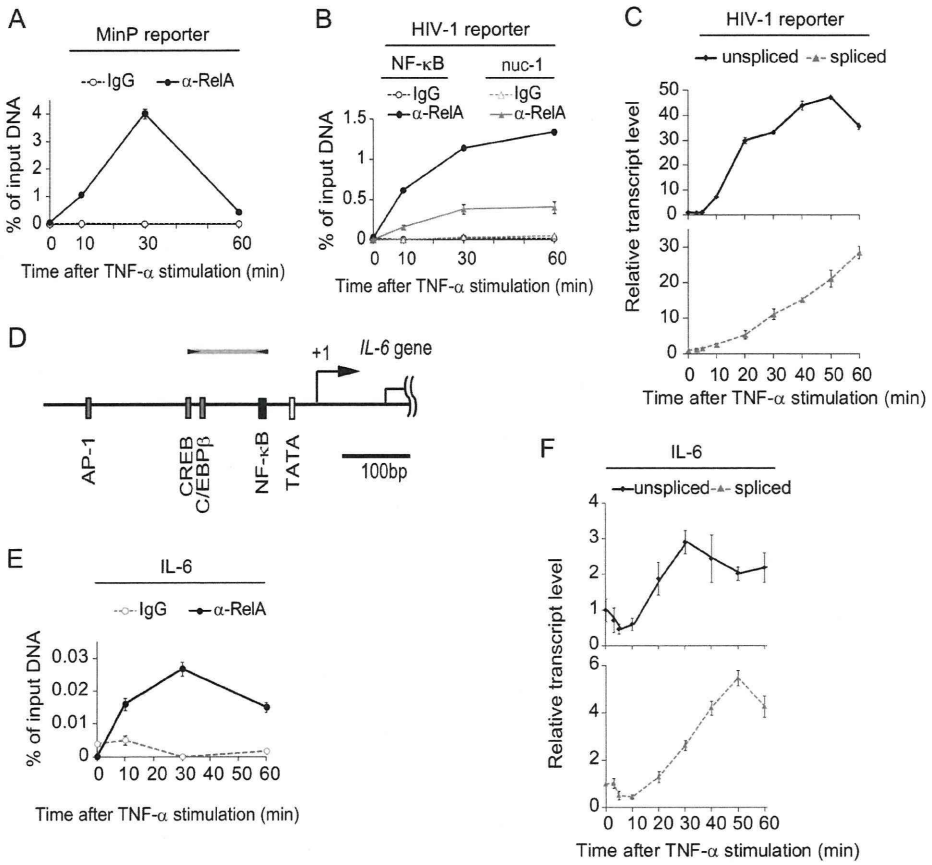

FIGURE 3. **Kinetics of RelA recruitment upon TNF-α stimulation correlate with the primary transcript production levels from both artificial and native promoters.** *A*, *B*, and *E*, kinetics of RelA recruitment to NF-κB-MinP (*A*), HIV-1 LTR (*B*), and the endogenous IL-6 promoter (*E*) upon TNF-α stimulation. Cells were treated with 10 ng/ml TNF-α for the indicated times and were harvested and precipitated by antibodies against RelA or with a normal rabbit IgG control. The immunoprecipitated DNA was quantified by real time PCR and normalized relative to the input. *C* and *F*, real time RT-PCR analysis of transcripts of HIV-1 LTR (*C*) and the endogenous IL-6 promoter (*F*). Cells were treated with 10 ng/ml TNF-α for the indicated times, and mRNA was prepared. Spliced and unspliced mRNAs were quantified, and these levels were normalized to individual untreated samples. *D*, schematic representation of the *IL-6* promoter region. The binding site for NF-κB and other transcription factors and the TATA box are highlighted by *black*, *gray*, and *white bars*, respectively. Transcriptional start sites are designated as +1. Positions detected by real time PCR are indicated by *black arrows* and a *gray bar*.

was previously reported at a single cell resolution that RelA oscillates dynamically between the nucleus and the cytoplasm and that this oscillation cycle is about 1 h (29). To analyze the primary effects of TNF-α stimulation on RelA/p50 transactivation, we performed ChIP analysis of the promoters of the reporter genes after stimulation within 1 h. In NF-κB-MinP-Luc-A3 cells, the results showed that the stimulation-dependent recruitment of RelA achieved a peak at 30 min post-treatment and drastically reduced to marginal levels within 60 min (Fig. 3*A*). Next, by using 293FT cells harboring an HIV-1-based reporter provirus (293FT-LTR-Luc-5; Fig. 1*B*) instead, we performed the same set of analyses (Fig. 3*B*). Interestingly, RelA recruitment to the NF-κB-responsive elements within the HIV-1 LTR kept increasing during the first 60 min after TNF-α stimulation with small leakage of the signal detected in the nucleosome 1 (nuc-1) region. Considering that the nucleotide sequences of the NF-κB elements are identical in both of these promoters, it is noteworthy that distinct kinetics of RelA recruitment were observed, *i.e.* the wild type HIV-1 LTR retains RelA longer.

We next analyzed whether there was any association between the recruitment levels of RelA and the transactivation kinetics of these promoters. By quantifying the HIV-1 LTR transcript levels at the indicated time points by real time RT-PCR, we found that the kinetics of the *de novo* synthesized primary unspliced mRNAs were very similar to those of RelA recruitment, whereas those of the mature spliced mRNAs kept increasing (Fig. 3*C*). Because the primary transcript of NF-κB-MinP does not contain introns, it cannot be distinguished from the mature mRNA. Interestingly, using a promoter of an endogenous TNF-α-inducible gene, IL-6 (Fig. 3*D*), which requires the SWI/SNF complex for activation (14), we observed a good correlation in kinetics between RelA recruitment and primary transcript synthesis after TNF-α stimulation (Fig. 3, *E* and *F*, and the induction kinetics is more prompt than those observed for HIV-1 LTR in the same cells (Fig. 3*B*). In addition, the kinetics of the recruitment of RelA to the *IL-6* promoter are similar to those of NF-κB-MinP, achieving a peak at 30 min after stimulation and decreasing at 60 min. Our present observations thus suggest that HIV-1 LTR retains RelA longer against the oscillation cycle of RelA between the nucleus and the cytoplasm. HIV-1 LTR contains many binding sites for other transcription factors, some of which would associate with RelA (30–32). This might cause differences in the kinetics of the

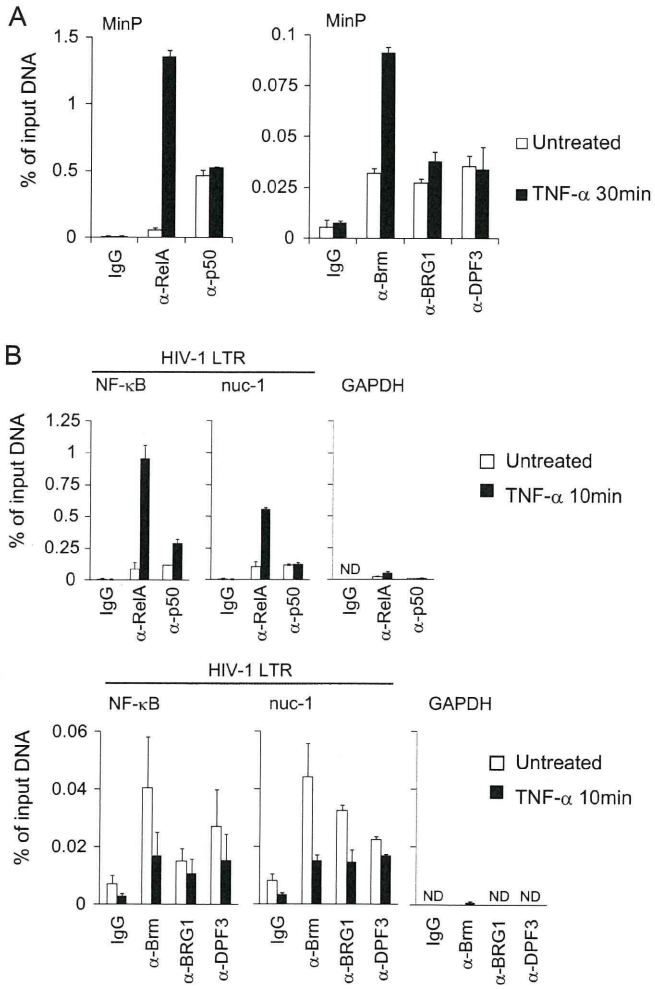

FIGURE 4. **Chromatin dynamics and recruitment of DPF3 and RelA/p50 to SWI/SNF-dependent promoters upon TNF-α treatment.** ChIP analysis was performed, and the data were quantified as described in Fig. 3. *A*, ChIP analysis of RelA, p50, Brm, BRG1, and DPF3 levels at the NF-κB-MinP upon TNF-α stimulation. *B*, recruitment of RelA, p50, Brm, BRG1, BAF60a, Ini1, and DPF3 to the regions within the HIV-1 LTR and GAPDH promoter after TNF-α treatment. Results presented here are the average of at least two independent experiments. *ND*, not detectable.

artificial MinP, which is simply under the control of NF-κB. However, the endogenous *IL-6* promoter is also regulated by other transcription regulators but showed no retention of RelA. This observation might be reflecting that, unlike HIV-1 LTR, this gene is expected to be strictly down-regulated after the stimulation for proper inflammatory response.

Chromatin Dynamics around the NF-κB-binding Sites in Both Artificial and Native Promoters after TNF-α Treatment—We next analyzed the dynamics of endogenous DPF3 and the SWI/SNF complex as well as RelA/p50 for both NF-κB-MinP and HIV-1 LTR in response to TNF-α stimuli. Consistent with Fig. 3*A*, this stimulation caused a dynamic recruitment of RelA to NF-κB-MinP at 30 min (*left panel* of Fig. 4*A*). Similar amounts of NF-κB p50 subunit were detected both before and after TNF-α stimulation, which we think is consistent with previous observations that low levels of the p50 subunit are present on specific NF-κB-responsive promoters in the nucleus of unstimulated cells as the p50 homodimer, whereas the majority of this subunit is retained in the cytoplasm as RelA/p50 (33–35). The p50 homodimer itself does not contain transactivation domains, but it associates with promoter regions of some NF-κB-dependent genes, including integrated HIV-1 LTR in the unstimulated conditions (36). However, Brm, BRG1, and DPF3 were all detected at the promoter even before stimulation, and their recruitment levels were not significantly changed upon exposure to TNF-α, apart from Brm, which showed elevated levels at the promoter (*right panel* of Fig. 4*A*). In the case of 293FT-LTR-Luc-5 cells, RelA was recruited to NF-κB elements in the HIV-1 LTR within 10 min of stimulation, whereas the NF-κB p50 subunit was found to be constitutively present in the LTR (*upper panel* of Fig. 4*B*). Brm, BRG1, and DPF3 were also detected at the promoter prior to TNF-α treatment, and their recruitment levels were reduced by about 50% after stimulation, suggesting that upon transcriptional activation, the SWI/SNF complex partially releases from the promoter with DPF3 (*lower panel* of Fig. 4*B*). Because other subunits of the complex such as BAF60a and Ini1 behaved in a similar manner to Brm or BRG1 (supplemental Fig. S9), we speculate that the changes in the levels of the catalytic subunits associated with the HIV-LTR promoter were as part of the SWI/SNF complex.

Whereas the two promoters under analysis showed different RelA recruitment kinetics, they were found to share two important features from our observations. First, endogenous DPF3 together with the SWI/SNF complex is bound to the promoters prior to TNF-α stimulation. Second, upon stimulation, RelA/p50, which can directly interact with DPF3 (Fig. 2*A*), was found to be rapidly recruited to the promoters, and this recruitment was shown to be associated with transcriptional activation, as judged by the primary transcript levels.

Finally, we analyzed the endogenous *IL-6* promoter to check whether DPF3 links the SWI/SNF complex and RelA/p50 forming a larger complex. ChIP analysis showed that both RelA and DPF3a/b were recruited to the promoter in a TNF-α-dependent and -independent manner, respectively (Fig. 5*A*). To perform sequential ChIP analysis, the immunoprecipitates with α-RelA antibody were re-immunoprecipitated with antibodies specific for DPF3a/b and Brm as well as the α-RelA antibody (positive control) and normal rabbit IgG (negative control), respectively (Fig. 5*B*). The second round of immunoprecipitates using α-DPF3 and Brm antibodies indicated that DPF3 and the SWI/SNF complex co-associate with RelA on the *IL-6* promoter after the RelA/p50 heterodimer is recruited upon TNF-α stimulation. In conclusion, all these results support that DPF3a and -3b link the SWI/SNF complex to NF-κB to transactivate the target promoters that require chromatin remodeling for the transcriptional initiation.

DISCUSSION

By extending our previous observation that DPF2 links RelB/p52 and the SWI/SNF complex for NF-κB transactivation via its noncanonical pathway, we have here shown that each of the five proteins, DPF1, DPF2, DPF3a, DPF3b, and PHF10, can equally function as an efficient co-activator of the RelA/p50 dimer at the most downstream part of the NF-κB canonical pathway, when they are exogenously expressed at high levels

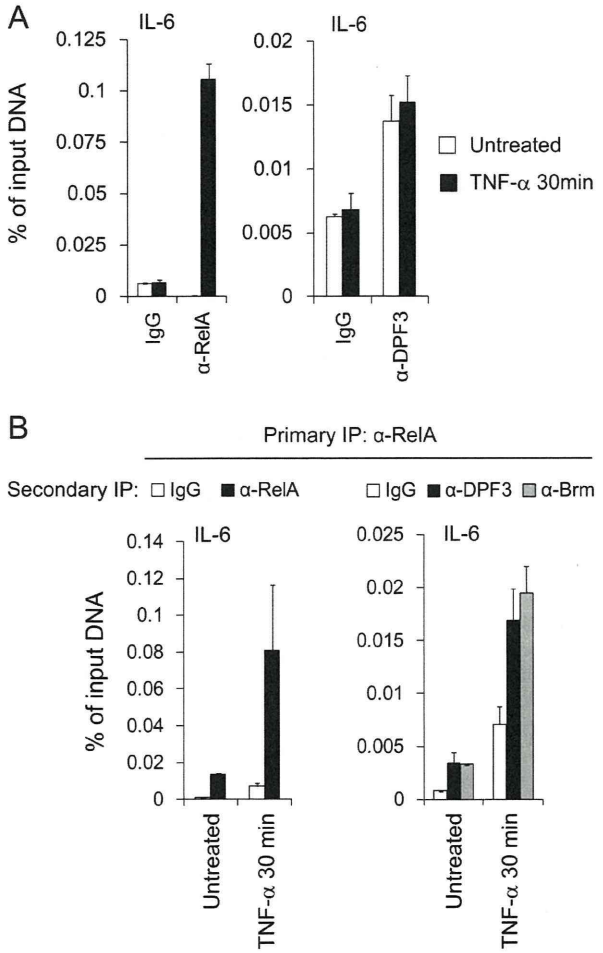

FIGURE 5. **ChIP and re-ChIP assays at the endogenous *IL-6* promoter.** *A,* ChIP analysis of RelA and DPF3 occupancy levels at the *IL-6* promoter. 293FT cells were treated with or without 10 ng/ml TNF-α for 30 min and harvested for precipitation by antibodies against RelA and DPF3. *B,* primary immunoprecipitated materials concentrated with α-RelA antibody were followed by secondary rounds of immunoprecipitations with indicated antibodies. Immunoprecipitated materials were quantified by real time PCR.

(Fig. 1*C*). Under these conditions, each of these proteins activated the other two representative NF-κB dimers, RelB/p52 and c-Rel/p50, with similar efficiencies. When these five proteins were expressed by retrovirus vectors, they are constitutively binding to the SWI/SNF complex in the nucleus and begin to associate with RelA/p50 upon TNF-α treatment (Fig. 2*C* and supplemental Fig. S8). From these results, we think each of these proteins would function as a co-activator of NF-κB in certain tissues. DPF1 was reported to be neurospecific and play an important role in developing neurons (20, 24). DPF2, which is ubiquitously expressed, is known to be involved in the processes of apoptosis in mouse myeloid cells following interleukin 3 (IL-3) deprivation (37). In normal cells, DPF3a/b was reported to be expressed specifically in cardiac and skeletal muscle and was critical for heart and muscle development (23). Because NF-κB plays important roles in programmed cell death and development, these d4 proteins might be involved in these physiological phenomena through activating some specific NF-κB dimers. Because DPF1, DPF2, DPF3b and PHF10 contain double PHD fingers, which are not possessed by any of the core subunits of the SWI/SNF complex, they are likely to play some roles in selecting specific species of modified histones in the nucleosomes at target promoter regions.

In 293FT cells, which express only low levels of endogenous mRNAs for the five candidate protein co-activators, the knockdown of either DPF3a or DPF3b suppressed TNF-α-induced NF-κB transactivation to marginal levels, suggesting that both proteins are essential for the NF-κB canonical pathway (Fig. 1*D*). Currently, we cannot fully explain this observation, but there could be several possibilities. One possibility would be that the SWI/SNF complex needs to bind both DPF3a and DPF3b to perform its full function for NF-κB transactivation. We would, however, prefer another possibility as follows. DPF3a and DPF3b share roles in NF-κB transactivation probably through their common N-terminal regions. The endogenous cellular amounts of both proteins in 293FT cells are so low (supplemental Fig. S3) that depletion of either would drastically reduce their recruitment frequency to the promoter of the reporter, where a single molecule of either DPF3a or DPF3b is sufficient for the SWI/SNF complex to perform full transactivation. Because DPF3a lacks functional PHD fingers, however, it is also possible that they would show distinct promoter preferences in some cases, as has been shown previously by ChIP analysis of exogenously expressed DPF3a and DPF3b (23).

We have previously shown that a representative target gene of the NF-κB canonical pathway, *IL-8,* is induced in HeLa cells by TNF-α and that this induction is not affected by the knockdown of DPF2. We suggested from this that DPF2 does not significantly contribute to the NF-κB canonical pathway, at least in this cell system. Because the endogenous *IL-8* gene was found not to be affected by the knockdown of either catalytic subunit of the SWI/SNF complex (19), we believe that this promoter is induced independently of SWI/SNF. In immune cells, some NF-κB target promoters have also been reported not to require chromatin remodeling for their transcriptional initiation upon LPS stimulation, because they already possess an open chromosome structure (38).

Importantly, with respect to our current investigations, the results of ChIP analysis using antiserum that we prepared indicated that the endogenous DPF3 proteins (this antiserum does not discriminate between DPF3a and DPF3b) as well as the SWI/SNF complex are recruited continuously to the promoters we examined, NF-κB-MinP and wild type HIV-1 LTR. Considering that both DPF3a and DPF3b directly bind to p50 *in vitro,* we speculate that DPF3a/3b together with the SWI/SNF complex locate near the NF-κB-binding sites through the binding of the p50 homodimer under unstimulated conditions but through active RelA/p50 upon stimulation. This dimer substitution would then trigger SWI/SNF-dependent transactivation. Hence, the SWI/SNF complex would be present at these target promoters to facilitate the ready recruitment of RelA/p50 for the prompt remodeling of the surrounding chromatin structures. Considering our observations that transcriptional enhancement of HIV-1 LTR occurs just after the SWI/SNF complex and RelA/p50 get together on the promoter (Figs. 3, *B* and *C,* and 4*B*), DPF3a/3b is significant for this activation as a linker protein.

Acknowledgments—We thank S. Kawaura and A. Kato for their assistance in preparing this manuscript. We thank Dr. H. Nakano and Dr. H. Watanabe for critical reading of this manuscript.

REFERENCES

1. Beinke, S., and Ley, S. C. (2004) Functions of NF-κB1 and NF-κB2 in immune cell biology. *Biochem. J.* **382,** 393–409
2. Santoro, M. G., Rossi, A., and Amici, C. (2003) NF-κB and virus infection. Who controls whom. *EMBO J.* **22,** 2552–2560
3. Vallabhapurapu, S., and Karin, M. (2009) Regulation and function of NF-κB transcription factors in the immune system. *Annu. Rev. Immunol.* **27,** 693–733
4. Ben-Neriah, Y., and Karin, M. (2011) Inflammation meets cancer, with NF-κB as the matchmaker. *Nat. Immunol.* **12,** 715–723
5. Gilmore, T. D. (2006) Introduction to NF-kappaB: players, pathways, perspectives. *Oncogene* **25,** 6680–6684
6. Ghosh, S., May, M. J., and Kopp, E. B. (1998) NF-κB and Rel proteins. Evolutionarily conserved mediators of immune responses. *Annu. Rev. Immunol.* **16,** 225–260
7. Pomerantz, J. L., and Baltimore, D. (2002) Two pathways to NF-κB. *Mol. Cell* **10,** 693–695
8. Muchardt, C., and Yaniv, M. (1999) ATP-dependent chromatin remodeling. SWI/SNF and Co. are on the job. *J. Mol. Biol.* **293,** 187–198
9. Wilson, B. G., and Roberts, C. W. (2011) SWI/SNF nucleosome remodelers and cancer. *Nat. Rev. Cancer* **11,** 481–492
10. Kwon, H., Imbalzano, A. N., Khavari, P. A., Kingston, R. E., and Green, M. R. (1994) Nucleosome disruption and enhancement of activator binding by a human SWI/SNF complex. *Nature* **370,** 477–481
11. Cheng, S. W., Davies, K. P., Yung, E., Beltran, R. J., Yu, J., and Kalpana, G. V. (1999) c-MYC interacts with INI1/hSNF5 and requires the SWI/SNF complex for transactivation function. *Nat. Genet.* **22,** 102–105
12. Kowenz-Leutz, E., and Leutz, A. (1999) A C/EBPβ isoform recruits the SWI/SNF complex to activate myeloid genes. *Mol. Cell* **4,** 735–743
13. Ito, T., Yamauchi, M., Nishina, M., Yamamichi, N., Mizutani, T., Ui, M., Murakami, M., and Iba, H. (2001) Identification of SWI.SNF complex subunit BAF60a as a determinant of the transactivation potential of Fos/Jun dimers. *J. Biol. Chem.* **276,** 2852–2857
14. Watanabe, H., Mizutani, T., Haraguchi, T., Yamamichi, N., Minoguchi, S., Yamamichi-Nishina, M., Mori, N., Kameda, T., Sugiyama, T., and Iba, H. (2006) SWI/SNF complex is essential for NRSF-mediated suppression of neuronal genes in human nonsmall cell lung carcinoma cell lines. *Oncogene* **25,** 470–479
15. Yamamichi, N., Inada, K., Furukawa, C., Sakurai, K., Tando, T., Ishizaka, A., Haraguchi, T., Mizutani, T., Fujishiro, M., Shimomura, R., Oka, M., Ichinose, M., Tsutsumi, Y., Omata, M., and Iba, H. (2009) Cdx2 and the Brm-type SWI/SNF complex cooperatively regulate villin expression in gastrointestinal cells. *Exp. Cell Res.* **315,** 1779–1789
16. Iba, H., Mizutani, T., and Ito, T. (2003) SWI/SNF chromatin remodeling complex and retroviral gene silencing. *Rev. Med. Virol.* **13,** 99–110
17. Mizutani, T., Ito, T., Nishina, M., Yamamichi, N., Watanabe, A., and Iba, H. (2002) Maintenance of integrated proviral gene expression requires Brm, a catalytic subunit of SWI/SNF complex. *J. Biol. Chem.* **277,** 15859–15864
18. Mizutani, T., Ishizaka, A., Tomizawa, M., Okazaki, T., Yamamichi, N., Kawana-Tachikawa, A., Iwamoto, A., and Iba, H. (2009) Loss of the Brm-type SWI/SNF chromatin remodeling complex is a strong barrier to the Tat-independent transcriptional elongation of human immunodeficiency virus type 1 transcripts. *J. Virol.* **83,** 11569–11580
19. Tando, T., Ishizaka, A., Watanabe, H., Ito, T., Iida, S., Haraguchi, T., Mizutani, T., Izumi, T., Isobe, T., Akiyama, T., Inoue, J., and Iba, H. (2010) Requiem protein links RelB/p52 and the Brm-type SWI/SNF complex in a noncanonical NF-κB pathway. *J. Biol. Chem.* **285,** 21951–21960
20. Buchman, V. L., Ninkina, N. N., Bogdanov, Y. D., Bortvin, A. L., Akopian, H. N., Kiselev, S. L., Krylova OYu., Anokhin, K. V., and Georgiev, G. P. (1992) Differential splicing creates a diversity of transcripts from a neuro-specific developmentally regulated gene encoding a protein with new zinc finger motifs. *Nucleic Acids Res.* **20,** 5579–5585
21. Chestkov, A. V., Baka, I. D., Kost, M. V., Georgiev, G. P., and Buchman, V. L. (1996) The d4 gene family in the human genome. *Genomics* **36,** 174–177
22. Ninkina, N. N., Mertsalov, I. B., Kulikova, D. A., Alimova-Kost, M. V., Simonova, O. B., Korochkin, L. I., Kiselev, S. L., and Buchman, V. L. (2001) Cerd4, third member of the d4 gene family. Expression and organization of genomic locus. *Mamm. Genome* **12,** 862–866
23. Lange, M., Kaynak, B., Forster, U. B., Tönjes, M., Fischer, J. J., Grimm, C., Schlesinger, J., Just, S., Dunkel, I., Krueger, T., Mebus, S., Lehrach, H., Lurz, R., Gobom, J., Rottbauer, W., Abdelilah-Seyfried, S., and Sperling, S. (2008) Regulation of muscle development by DPF3, a novel histone acetylation and methylation reader of the BAF chromatin remodeling complex. *Genes Dev.* **22,** 2370–2384
24. Lessard, J., Wu, J. I., Ranish, J. A., Wan, M., Winslow, M. M., Staahl, B. T., Wu, H., Aebersold, R., Graef, I. A., and Crabtree, G. R. (2007) An essential switch in subunit composition of a chromatin remodeling complex during neural development. *Neuron* **55,** 201–215
25. Chaturvedi, M. M., Sung, B., Yadav, V. R., Kannappan, R., and Aggarwal, B. B. (2011) NF-κB addiction and its role in cancer. "One size does not fit all." *Oncogene* **30,** 1615–1630
26. Perkins, N. D. (2006) Post-translational modifications regulating the activity and function of the nuclear factor κB pathway. *Oncogene* **25,** 6717–6730
27. Schmitz, M. L., Mattioli, I., Buss, H., and Kracht, M. (2004) NF-κB. A multifaceted transcription factor regulated at several levels. *ChemBioChem* **5,** 1348–1358
28. Viatour, P., Merville, M. P., Bours, V., and Chariot, A. (2005) Phosphorylation of NF-κB and IκB proteins. Implications in cancer and inflammation. *Trends Biochem. Sci.* **30,** 43–52
29. Nelson, D. E., Ihekwaba, A. E., Elliott, M., Johnson, J. R., Gibney, C. A., Foreman, B. E., Nelson, G., See, V., Horton, C. A., Spiller, D. G., Edwards, S. W., McDowell, H. P., Unitt, J. F., Sullivan, E., Grimley, R., Benson, N., Broomhead, D., Kell, D. B., and White, M. R. (2004) Oscillations in NF-κB signaling control the dynamics of gene expression. *Science* **306,** 704–708
30. Stevens, M., De Clercq, E., and Balzarini, J. (2006) The regulation of HIV-1 transcription. Molecular targets for chemotherapeutic intervention. *Med. Res. Rev.* **26,** 595–625
31. Rohr, O., Marban, C., Aunis, D., and Schaeffer, E. (2003) Regulation of HIV-1 gene transcription. From lymphocytes to microglial cells. *J. Leukocyte Biol.* **74,** 736–749
32. Pereira, L. A., Bentley, K., Peeters, A., Churchill, M. J., and Deacon, N. J. (2000) A compilation of cellular transcription factor interactions with the HIV-1 LTR promoter. *Nucleic Acids Res.* **28,** 663–668
33. Satou, R., Miyata, K., Katsurada, A., Navar, L. G., and Kobori, H. (2010) Tumor necrosis factor-α suppresses angiotensinogen expression through formation of a p50/p50 homodimer in human renal proximal tubular cells. *Am. J. Physiol. Cell Physiol.* **299,** C750–C759
34. Wu, Z. Z., Chow, K. P., Kuo, T. C., Chang, Y. S., and Chao, C. C. (2011) Latent membrane protein 1 of Epstein-Barr virus sensitizes cancer cells to cisplatin by enhancing NF-κB p50 homodimer formation and down-regulating NAPA expression. *Biochem. Pharmacol.* **82,** 1860–1872
35. Zhong, H., May, M. J., Jimi, E., and Ghosh, S. (2002) The phosphorylation status of nuclear NF-κB determines its association with CBP/p300 or HDAC-1. *Mol. Cell* **9,** 625–636
36. Williams, S. A., Chen, L. F., Kwon, H., Ruiz-Jarabo, C. M., Verdin, E., and Greene, W. C. (2006) NF-κB p50 promotes HIV latency through HDAC recruitment and repression of transcriptional initiation. *EMBO J.* **25,** 139–149
37. Gabig, T. G., Mantel, P. L., Rosli, R., and Crean, C. D. (1994) Requiem. A novel zinc finger gene essential for apoptosis in myeloid cells. *J. Biol. Chem.* **269,** 29515–29519
38. Ramirez-Carrozzi, V. R., Braas, D., Bhatt, D. M., Cheng, C. S., Hong, C., Doty, K. R., Black, J. C., Hoffmann, A., Carey, M., and Smale, S. T. (2009) A unifying model for the selective regulation of inducible transcription by CpG islands and nucleosome remodeling. *Cell* **138,** 114–128

1944–1953 *Nucleic Acids Research, 2012, Vol. 40, No. 5* *Published online 10 November 2011*
doi:10.1093/nar/gkr979

Functional and direct interaction between the RNA binding protein HuD and active Akt1

Toshinobu Fujiwara[1,*], Akira Fukao[2], Yumi Sasano[3], Hidenori Matsuzaki[4], Ushio Kikkawa[4], Hiroaki Imataka[5], Kunio Inoue[2], Shogo Endo[6], Nahum Sonenberg[7], Christian Thoma[8,*] and Hiroshi Sakamoto[2,*]

[1]Laboratory of Disease Biology, Institute of Microbial Chemistry, 3-14-23 Kamiosaki, Shinagawa-ku, Tokyo 141-0021, [2]Department of Biology, Graduate School of Science, Kobe University, [3]Research & Development Center, Nagase & Co., Ltd. 2-2-3 Murotani, Nishi-ku, Kobe, Hyogo 651-2241, [4]Biosignal Research Center Kobe University, 1-1 Rokkodaicho, Nada-ku, Kobe 657-8501, [5]Department of Materials Science and Chemistry, Graduate School of Engineering, University of Hyogo, Himeji 671-2280, [6]Aging Regulation Research Team, Tokyo Metropolitan Institute of Gerontology, Itabashi, Tokyo 173-0015, Japan, [7]Department of Biochemistry and McGill Cancer Centre, McGill University, Montreal, Quebec, H3G 1Y6, Canada and [8]Department of Medicine II, University Hospital of Freiburg, Hugstetterstr 55, 79106 Freiburg, Germany

Received June 29, 2011; Revised and Accepted October 14, 2011

ABSTRACT

The RNA binding protein HuD plays essential roles in neuronal development and plasticity. We have previously shown that HuD stimulates translation. Key for this enhancer function is the linker region and the poly(A) binding domain of HuD that are also critical for its function in neurite outgrowth. Here, we further explored the underlying molecular interactions and found that HuD but not the ubiquitously expressed HuR interacts directly with active Akt1. We identify that the linker region of HuD is required for this interaction. We also show by using chimeric mutants of HuD and HuR, which contain the reciprocal linker between RNA-binding domain 2 (RBD2) and RBD3, respectively, and by overexpressing a dominant negative mutant of Akt1 that the HuD–Akt1 interaction is functionally important, as it is required for the induction of neurite outgrowth in PC12 cells. These results suggest the model whereby RNA-bound HuD functions as an adapter to recruit Akt1 to trigger neurite outgrowth. These data might also help to explain how HuD enhances translation of mRNAs that encode proteins involved in neuronal development.

INTRODUCTION

RNA binding proteins (RBPs) are key mediators of post-transcriptional control mechanisms, including the control of mRNA translation (1,2). This cytoplasmic regulatory mechanism also plays crucial roles in neuronal development (2). Several RBPs are specifically expressed in neurons such as the neuronal Hu proteins, which are essential for proper neuronal development and plasticity (3). The neuronal Hu family consists of three members, HuB, HuC and HuD. Hu proteins contain three RNA-binding domains (RBDs) and a linker region between RBD2 and RBD3 (3). The biological functions of Hu proteins result from their ability to bind to target mRNAs. Hu proteins stabilize adenine/uridine-rich element (ARE)-containing transcripts by binding to AREs via RBD1 and RBD2 and also affect translation (3). We have recently shown that HuD upregulates cap- and poly(A)-dependent translation through a direct interaction with eukaryotic initiation factor 4A (eIF4A) via its linker region (4). This enhancer function also involves the poly(A) binding activity of HuD via RBD3 (4). Interestingly, the linker region and RBD3 are also crucial for the stimulatory effect of HuD on neurite outgrowth, revealing a posttranscriptional role in neuronal development and plasticity (4). However, the underlying molecular mechanism(s) and interactions are poorly understood. In

*To whom correspondence should be addressed. Tel:/Fax: +81 3 3441 5375; Email: tosinobu@bikaken.or.jp
Correspondence may also be addressed to Christian Thoma. Tel:/Fax: +49 761 27032770; Email: christian.thoma@uniklinik-freiburg.de
Correspondence may also be addressed to Hiroshi Sakamoto. Tel: +81 78 803 5796; Fax: +81 78 803 5720; Email: hsaka@kobe-u.ac.jp
Present address:
Hidenori Matsuzaki, Department of Hygiene Kawasaki Medical School, 577 Matsushima, Kurashiki, Okayama 701-0192, Japan.

The authors wish it to be known that, in their opinion, the first two authors should be regarded as joint First Authors

particular, little is known about the involved signaling components. The phosphatidylinositol 3-kinase (PI3K)/Akt1 pathway is one of the major signaling transduction cascades regulating translation (5). Activated PI3K leads to an activation of Akt1. Activated Akt1 regulates protein synthesis via mammalian Target Of Rapamycin (mTOR) by targeting ribosomal protein S6 and multiple initiation factors including the components of the eIF4F complex. Interestingly, Akt1 signaling is also involved in the neurite outgrowth mechanism induced by nerve growth factor (NGF) (6). Here, we report that RNA-bound HuD interacts specifically and directly with active Akt1 to induce neurite outgrowth. We identify the linker region between RBD2 and RBD3 as the binding domain and show that the HuD–Akt1 interaction is functionally relevant as it is required for HuD-triggered neurite outgrowth in PC12 cells.

MATERIALS AND METHODS

Plasmids

Plasmids encoding T7-tagged mouse HuD proteins and glutathione-S-transferase (GST)-HuD fusion proteins were described previously (7,8). To generate the chimeric constructs FLAG-HuR-DL and FLAG-HuD-RL, the HuD- or HuR-linker, respectively, was inserted into the pFLAG HuR and HuD constructs. pFLAG-Akt1 dn was generated from pFLAG-Akt1 by replacing Lys179, Thr308 and Ser473 with Ala, using the QuikChange Site-Directed Mutagenesis Kit (Stratagene) (9,10).

Recombinant proteins

Hu proteins expressed in *Escherichia coli* as GST-fusions were purified as described (7,8). Recombinant active and inactive Akt1 were purchased from Upstate (Millipore).

Purification of FLAG-Akt1 and FLAG-eIF4B

HeLa cells were transfected with the expression plasmid coding for FLAG-tagged Akt1 or FLAG-tagged eIF4B and cultured for 48 h at 37°C. The purification procedures were carried out on ice. The extract from HeLa cells (1×10^7 cells) was lysed in lysis buffer (20 mM Tris–HCl, pH 7.5 containing 1 mM EDTA, 1 mM EGTA, 10 mM 2-mercaptoethanol, 1% Triton X-100, 150 mM NaCl, 10 mM NaF, 1 mM Na3VO4 and 50 μg/ml phenylmethylsulfonylfluoride), treated with benzonase and centrifuged at 18 000*g* for 10 min. The supernatant was incubated with FLAG M2 affinity gel (Sigma) equilibrated with lysis buffer for 3 h. After washing resin, FLAG-Akt was eluted with 100 μl of elution buffer (20 mM Tris–HCl, 150 mM NaCl, 1 mM EGTA, 1 mM EDTA, 10 mM 2-mercaptoethanol, 50 μg/ml phenylmethylsulfonyl fluoride and 100 μg/ml 3× FLAG-peptide) (11).

Cell culture and transfection

PC12 and HeLa cells were cultured in Dulbecco's modified Eagle's medium (Gibco) supplemented with 10% fetal bovine serum and 5% horse serum (for PC12 cells) or 10% fetal bovine serum (for HeLa cells), respectively. Cells were transiently transfected using the Lipofectamine 2000 transfection reagent (Invitrogen).

Immunoprecipitation

HeLa cells that have been cotransfected with the constructs coding for T7-HuD or T7-GFP and FLAG-tagged Akt1 were lysed in TNE buffer (20 mM Tris–HCl, pH 7.5, 150 mM NaCl, 2 mM EDTA, 1% NP-40, 1 mM phenylmethylsulfonyl fluoride, 10 μg/ml aprotinin and 10 μg/ml leupeptin). The extracts were then used for immunoprecipitation. Anti-T7 monoclonal antibody (Novagen) or anti-FLAG polyclonal antibody (Sigma) was added to the extracts together with protein G–sepharose beads. Bound proteins were eluted with SDS–PAGE loading buffer and subjected to SDS–PAGE and western blotting using anti-T7 monoclonal antibody and anti-FLAG polyclonal antibody.

In vitro binding experiments

GST pull-down assays were performed in TNE buffer (composition see above) as described previously (8). Bound proteins were separated by SDS–PAGE. Immunoblotting (IB) was performed with anti-FLAG, anti-Akt1 polyclonal antibodies and anti-GST monoclonal antibody (Sigma).

Determination of neurite-inducing activity in PC12 cells

After transfection of PC12 cells with constructs coding for T7-tagged or FLAG-tagged proteins, cells were cultured for 3 days and immunostained with anti-T7 polyclonal antibody (Bethyl) and anti-α-tubulin monoclonal antibody (Sigma). To address the role of Akt1 on the neurite-inducing activity of HuD, PC12 cells were cotransfected with T7-HuD or HuR-DL and either Akt1 dn or wild-type Akt1 and incubated for 3 days at 37°C. Immunostaining was then performed with anti-T7 polyclonal antibody and anti-FLAG monoclonal antibody (Sigma). Alexa 488 anti-rabbit IgG and Alexa 546 anti-mouse IgG were used as secondary antibodies, 1:1000 dilution (Invitrogen). Confocal analysis was performed using a confocal laser-scanning microscope (Zeiss LSM5 Pascal).

GSK-3β protein kinase assay

The enzyme activity of Akt1 was assayed by measuring the incorporation of radioactivity from [γ-^{32}P] ATP to glycogen synthase kinase 3β (GSK-3β) fusion protein (cell signaling), a synthetic substrate specific to Akt. Active Akt1 (upstate) was incubated with purified GST-HuD, GST-HuR or GST. Next, poly(U) beads were added to the mixture and incubated for 120 min. The poly(U) beads were collected by centrifugation and washed three times with TNE buffer. Before the kinase assay, the collected precipitates were washed at 0–4°C with 20 mM Tris–HCl pH 7.5 containing 1 mM EDTA, 1 mM EGTA, 10 mM 2-mercaptoethanol, 150 mM NaCl and 50 μg/ml phenylmethylsulfonyl fluoride to remove NP-40. The reaction mixture (25 μl) containing 20 mM Tris–HCl, pH 7.5, 10 mM $MgCl_2$, 20 mM ATP, 15–50 kBq of [γ-^{32}P] ATP and 100 mg/ml GSK-3β fusion

protein was then added to the precipitates and incubated for 30 min at 30°C. After boiling in SDS sample buffer, phosphorylated proteins were separated by SDS–PAGE. The radioactivity of the GSK-3β fusion protein band was analyzed by Bio-imaging Analyzer BAS2500 (Fujix).

In vitro kinase reaction using GST-HuD, FLAG-eIF4B or MBP-FOXO4

GST-HuD, FLAG-eIF4B or maltose-binding protein (MBP)-FOXO4 (Forkhead box protein O4) were incubated with and without active Akt1 in 20 mM Tris–HCl, pH 7.5, 10 mM $MgCl_2$, 20 μM ATP and [γ-^{32}P] ATP at 30°C for 30 min. After boiling in SDS-sample buffer, proteins were separated by SDS–PAGE. ^{32}P-labeled proteins were visualized using Bio-imaging Analyzer, BAS2500(Fuji) after Coomassie Brilliant Blue (CBB) staining (12).

RESULTS

HuD directly interacts with active Akt1

To examine the mechanism of how HuD induces neurite outgrowth, we used PC12 cells, which are an established model system for studying neuronal differentiation (13,14). PC12 cells can be induced to form neurites by overexpression of HuD (15). Using this system, we have recently shown that the eIF4A- and poly(A)-binding domains of HuD contribute to its neurite-inducing activity (4). We have also shown that these activities are critical for stimulating cap-dependent translation. Here, we further investigated the underlying molecular interactions.

Activation of the mTOR pathway by PI3K-Akt signaling is key for stimulating translation. Akt signaling promotes growth and proliferation including NGF-mediated neurite outgrowth induction (6). We hypothesized that (i) Akt1 function might be critical for the neurite-inducing activity of HuD and (ii) Akt1 might directly interact with HuD to fulfill this function. To examine this possibility, we performed first immunoprecipitation assays using HeLa cell lysates expressing FLAG-tagged Akt1 and T7-tagged HuD or GFP (Figure 1). Indeed, HuD, but not the negative control GFP, copurifies with FLAG-Akt1 (Figure 1A, left panel) and vice versa Akt1 copurifies with T7-HuD, but not with the control T7-GFP (Figure 1A, right panel).

To further confirm the interaction between endogenous Akt1 and HuD, we performed immunoprecipitation assays using PC12 cell lysates expressing T7-tagged HuD or GFP (Figure 1B) and examined coprecipitation of endogenous Akt1 with T7-tagged HuD or GFP. We found that endogenous Akt1 coimmunoprecipitated with T7-HuD but not with T7-GFP (Figure 1B).

Next, we tested whether the interaction is direct and specific or mediated by bridging RNA. To that end, we performed GST pull-down assays using purified recombinant GST-HuD and FLAG-tagged Akt1, which has been purified via FLAG M2 affinity gel (see 'Materials and Methods' section for further details) from benzonase-treated HeLa extracts before the GST pull-down assays (Figure 2A). We have used the endonuclease benzonase because it works well also at low temperatures and degrades all forms of RNA importantly also poly(A) RNA which is not digested by RNAse A. We found that FLAG-Akt1 copurifies with GST-HuD but not with the negative control GST (Figure 2A). Thus, the interaction between Akt1 and HuD is direct and specific.

To test whether active (phosphorylated) or inactive Akt1 interacts with HuD, we used commercially available

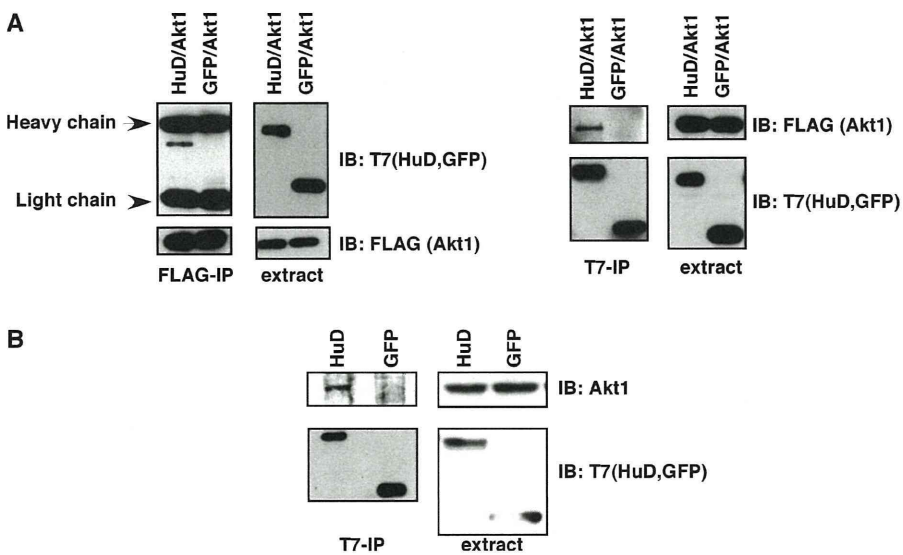

Figure 1. Protein–protein interaction by HuD and Akt1. (**A**) Specific coimmunoprecipitation of Akt1 with HuD. HeLa cells were transfected with T7-HuD or T7-GFP and FLAG-Akt1-coding plasmids. HuD was immunoprecipitated with anti-T7 antibody (right panel). Akt1 was immunoprecipitated with anti-FLAG antibody (left panel). Coimmunoprecipitation was monitored by IB. GFP is a negative control. (**B**) Specific coimmunoprecipitation of endogenous Akt1 with HuD. PC12 cells were transfected with T7-HuD- or T7-GFP-coding plasmids. HuD was immunoprecipitated with anti-T7 antibody. Coimmunoprecipitation of endogenous Akt1 was monitored by IB using anti-Akt1 antibodies.